WILEY

RESEARCH ARTICLE OPEN ACCESS

Greenhouse Gas Production and Microbial Response During the Transition From Terrestrial Permafrost to a Marine Environment

Maren Jenrich[1,2] | Michael Angelopoulos[1] | Susanne Liebner[3,4] | Claire Treat[1,2] | Christian Knoblauch[5,6] | Sizhong Yang[3] | Guido Grosse[1,2] | Fiona Giebeler[1,2] | Loeka L. Jongejans[1] | Mikhail Grigoriev[7] | Jens Strauss[1]

[1]Permafrost Research Section, Alfred Wegener Institute Helmholtz Centre for Polar and Marine Research, Potsdam, Germany | [2]Institute of Geosciences, University of Potsdam, Potsdam, Germany | [3]Section Geomicrobiology, GFZ German Research Centre for Geosciences, Potsdam, Germany | [4]Institute of Biochemistry and Biology, University of Potsdam, Potsdam, Germany | [5]Institute of Soil Sciences, Faculty of Mathematics, Informatics and Natural Sciences, Universität Hamburg, Hamburg, Germany | [6]Center for Earth System Research and Sustainability, Universität Hamburg, Hamburg, Germany | [7]Melnikov Permafrost Institute, Russian Academy of Sciences, Siberian Branch, Yakutsk, Russia

Correspondence: Maren Jenrich (maren.jenrich@awi.de)

ABSTRACT

Arctic permafrost coasts, affected by rising sea levels and increasing coastal erosion in a warming climate, undergo significant changes. Simulating how permafrost is impacted by inundation with fresh, brackish and marine water enhances our understanding of permafrost carbon stock responses to increasingly marine conditions. We investigated CO_2 and CH_4 production during key transitions in a coastal thermokarst landscape on the Bykovsky Peninsula, Siberia, assessing short- and long-term microbial responses to varying salinities in anaerobic 1-year incubation experiments. Initially, CO_2 production from saltwater-inundated permafrost was low due to the low abundance of salt-tolerant microbial communities. Over the long term, after simulated lagoon formation and the growth of sulfate-reducing bacteria, CO_2 production surpassed that of the terrestrial sites by 8 times. CO_2 and CH_4 production was lowest under fully marine conditions, suggesting incomplete adaptation of microbes. Rapid ecosystem changes stress microbial communities, with greenhouse gas production highest under near-natural conditions. With an increase in lake drainage events and rising sea levels, thermokarst lagoon distribution on Arctic coasts will escalate, resulting in a further increase of carbon mineralization and CO_2 release. With this study, we provide first estimations on greenhouse gas production during the transition from terrestrial to submarine conditions in permafrost-affected aquatic systems.

1 | Introduction

Approximately 15% of the land area of the Northern Hemisphere [1] and about 80% of the Arctic Beaufort, Chukchi, East Siberian, Laptev, and Kara Seas [2] are underlain by permafrost. The terrestrial permafrost (TPF) area is estimated to contain a reservoir of 1700 petagrams (Pg; 10^{15} g) of organic carbon (OC) deposited in frozen soil, the active layer [3–5], and onshore taliks [6, 7], in addition to 2800 Pg of OC below the seafloor [8]. The Arctic is warming nearly four times faster than the global average [9], and so, the TPF is thawing. Subsea permafrost is already in thermal disequilibrium because of the overlying seawater, but warming shelf waters and a shrinking sea ice extent can increase the thawing rate [10]. Permafrost thawing unlocks

ancient organic matter (OM), which can be decomposed by microorganisms into greenhouse gases (GHG) such as carbon dioxide (CO_2) and methane (CH_4), further fueling the warming of the Earth's climate. During winter, the TPF region loses 1.66 Pg OC in the form of CO_2 from Arctic and boreal soils [11]. This is higher than the carbon uptake during the growing season in summer, converting the terrestrial Arctic into a carbon source [4]. In contrast, subsea permafrost thaw is more resistant to climate warming and OM decomposition rates are lower, in part because the OM has already been exposed to multiple marine transgression and regression cycles [8].

The thaw of ice-rich permafrost is causing substantial land surface subsidence. This process is called thermokarst and leads to the formation of thermokarst features such as ponds, lakes, drained lake basins, and lagoons. Thermokarst lagoons form when thermokarst lakes or basins with bottom elevations below the sea level are breached along Arctic coasts by the sea due to coastal erosion [12–14] and sea-level rise [15–18] or become connected to the sea by their drainage channels [19]. Because of continued high rates of coastal erosion along ice-rich permafrost coasts [13, 20], thermokarst lagoons are transitional and dynamic coastal landforms that combine traits of both terrestrial and over time increasingly marine systems [19, 21–24]. The connectivity with the sea and thus water and sediment exchange is dependent on the size of the inlet and the ice dynamics of the inlet. The degree of connectivity has an impact on the physicochemical state (for example, salinity, ionic composition, temperature, turbidity, and nutrients) [23], the erodibility of the shore, and therefore also the mobilization of soil OC from land to the ocean. Lagoons with a narrow inlet channel (nearly closed lagoons) are characterized by a low exchange with sea water and have lower salt concentrations in the water in summer than more open lagoons (semi-open/open lagoons) [19]. With increasing connectivity, surface water salinity increases from brackish to marine conditions. When seawater enters a freshwater system, the ionic composition of surface and pore water is changing, altering the environmental conditions for macroorganisms and microorganisms. In the case of nearly closed lagoons, ice formation in winter can temporarily seal off the inlet and disconnect the lagoon from the sea [19, 25]. Within lagoons, salt diffuses into the sediment, forming unfrozen and saline ground [19, 26]. Beneath shallow lagoons, hypersalinity can develop in the sediment when bedfast ice injects salts into the sediment [19]. Since lagoon ice formation expels salts into the underlying liquid water, the salinity of the sediment can become much higher than the lagoon water salinity at the onset of freeze. Thus, shallow lagoons are niche environments in which only highly salt tolerant microorganisms (halophiles) survive.

So far, there is only a limited understanding of how carbon cycling behaves under the complex hydrochemical conditions in such coastal transitional environments. With the help of incubation experiments, it is possible to mimic OM decomposition processes and to measure the production of CO_2 and CH_4 in the course of landscape changes under laboratory conditions (e.g., [27, 28]). The decomposition of OM is influenced by various factors, including the OC content [29, 30], quality of OM [31], temperature [32], salinity, and the availability of oxygen [27, 32] within the soil. Previously, a simulation of an Arctic coastal erosion setting was achieved by incubating permafrost from a coastal outcrop with seawater, for 120 days, which approximates the time of an average Arctic open-water season [28]. The results demonstrated that the production of CO_2 from permafrost OC remains equally high under freshwater and marine conditions, which indicates that at least under these specific laboratory conditions, salinity does not significantly reduce CO_2 production.

While many studies focus on GHG production in soils from TPF and thermokarst landscapes [29, 31, 33–39], only little is known about OC decomposition, GHG production, and changes in microbial communities during the transition from land to subsea permafrost and subsequent thaw.

Especially in marine environments, sulfate-reducing microorganisms, such as sulfate-reducing bacteria (SRB) and sulfate-dependent archaea, use sulfate as electron acceptors to produce sulfide (S^{2-}) or to oxidize CH_4. Since sulfate-reducers outcompete methanogens under elevated sulfate concentrations, CH_4 production in marine, sulfate-containing sediments is generally low [40–44]. During lagoon formation, seawater intrusion introduces sulfate ions (SO_4^{2-}) into former freshwater lake or permafrost environments, likely resulting in complex changes of CH_4 production, oxidation, and emissions from these settings. For example, when sulfate is depleted, methanogenic archaea may increase their activity, leading to increased methane production. The net effect of seawater intrusion on methane emissions depends on the balance between sulfate reduction and methanogenesis. The presence of sulfate in permafrost environments can stimulate the activity of sulfate-reducing microorganisms, leading to changes in microbial community composition and metabolic activities [24, 45, 46].

The OM inventory of Arctic coastal areas is thus potentially exposed to large thermal and chemical changes with so far unknown consequences on GHG production. In our study, we are simulating the CO_2 and CH_4 production during the most important direct transitions that occur in a coastal thermokarst landscape: (I, II) ice-bonded permafrost transitioning into a thermokarst lake, a thermokarst lagoon, or into the subsea environment through block erosion; (III) thermokarst lakes transitioning into lagoons of different salinities; and (IV) lagoons becoming part of the shelf by using controlled laboratory incubation experiments. With that, we aim to answer the question: What is the potential local response of anaerobic CO_2 and CH_4 production to salinity changes in the short and in the long term? In our approach, we monitored CO_2 and CH_4 concentrations in 1-year long anaerobic incubations (short-term response) of sediment samples from TPF, lake, and lagoons under different salt concentrations (freshwater, brackish, and marine) and compared the microbial communities before and after the incubation. By using a space-for-time approach studying terrestrial aquatic systems and lagoons of different age and levels of connectivity, we mimic the long-term response to an increasingly marine influence.

2 | Study Area

The Bykovsky Peninsula is located southeast of the Lena Delta in the Buor-Khaya Gulf of the Laptev Sea in northeastern Siberia, Russia (Figure 1a). The peninsula is covered by
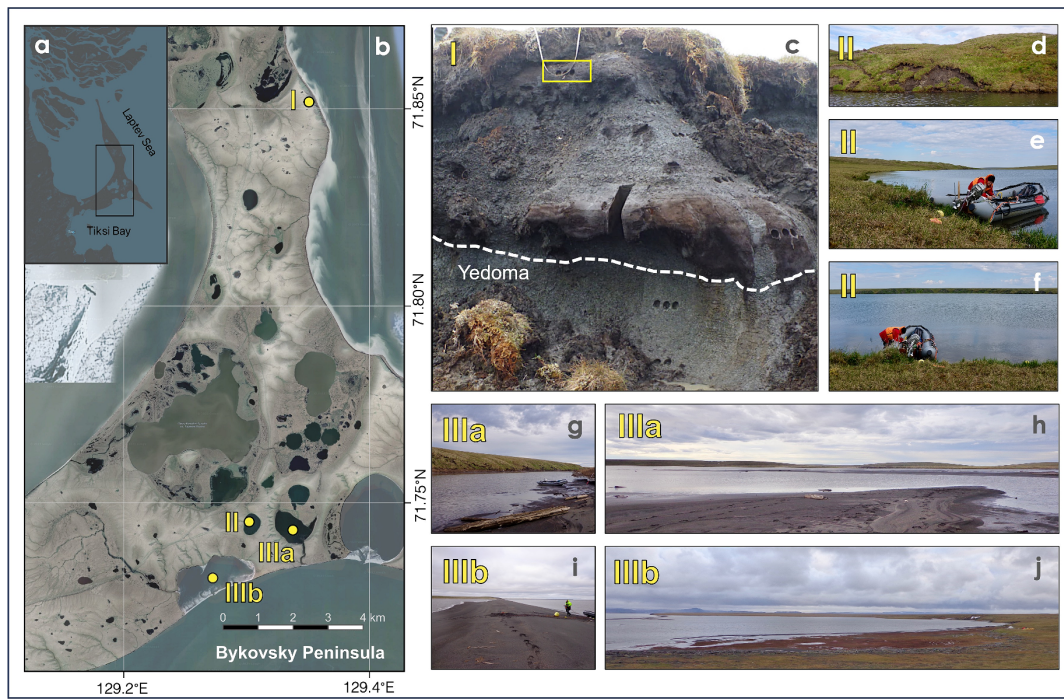
FIGURE 1 | Study sites located on the Bykovsky Peninsula in Northeast Siberia, southeast of the Lena Delta (a). Close-up of central Bykovsky Peninsula, coring locations are marked by a dot (b)—I: Permafrost outcrop (TPF) located at an Upland on the West Coast, three replicate coring locations in thermokarst deposits overlying Yedoma marked by the yellow rectangle (c); II: Thermokarst Lake Goltsovoye (TKL) (d, e, f), drilling occurred about 60 m offshore; IIIa: nearly closed thermokarst lagoon Polar Fox (LAG1) temporarily connected to the sea in summer by a channel (g, h) and IIIb: semi-open lagoon Uomullyakh (LAG2) separated by a sand barrier (i, j) with a small inlet are located in close distance to each other on the southern coast of the peninsula. Imagery sources: (a) ESRI base map; (b) satellite map is a combination of Google Satellite Hybrid base map and a hillshade map derived from the stereophotogrammetric DEM 3epipolar based on WorldView imagery from 2015; (c) photo by G. Grosse in summer 2014; photos (d–j) by M. Angelopoulos in summer 2017.

largely fine-grained deposits of the late Pleistocene, ice-rich Yedoma, and by Holocene thermokarst lake and basin sediments [47–49]. Thermokarst processes resulting from thaw of these ice-rich deposits play a significant role in shaping the landscape in this region, with thermokarst lakes covering approximately 15% of the peninsula [50] and thermokarst-affected areas, including drained lake basins, making up over 50% of the total land area [51]. The presence of Yedoma uplands, thermokarst depressions, and thermal erosional valleys contribute to the diverse topography of the Bykovsky Peninsula.

We chose a TPF outcrop located at the west coast (sampled in 2014) and three sediment cores below water bodies (cored in 2017) located at the south coast of the peninsula for our investigation (Figure 1b).

The outcrop TPF (71.85175° N, 129.350883° E; Figure 1b,c) is located on the headwall of a retrogressive thaw slump eroding into a Yedoma upland on the northwestern coast of the peninsula. The exposure contains 2.9 m of nearly vertically exposed ice-rich terrestrial sediments. The lowest exposed portion consists of Yedoma with gray ice-rich silts with reticulated (vertical and horizontal ice veins) to ataxitic (suspended sediment) cryostructure and some fine grass rootlets. Above this, a horizon of 30- to 60-cm thickness contains brown sedge peat overlain by a cryoturbated paleosoil horizon, indicating initial thermokarst development on the original Yedoma upland (so-called Bylary,

small thermokarst pits). The following organic-rich deposits all belong to this type of initial thermokarst development forming as cover deposits on Yedoma uplands. They include mixtures of brownish-gray ice-rich silt with reticulated cryostructure, small and large peat inclusions, small woody remains, and rootlets. Below the terrain surface, another 20- to 30-cm organic-rich silt layer with peat inclusions was found, which was overlain by a cryoturbated brownish-gray mineral-rich layer and a ~8-cm thin layer of Sphagnum moss representing the soil surface organic layer. The active layer at this location was about 0.3 m thick. The uppermost samples from this exposure from 0.3 to 0.35 m in depth serve as the terrestrial endmember for the three thermokarst settings (see Figure 1c).

The Thermokarst Lake Goltsovoye (TKL) (71.74515° N, 129.30217° E; Figure 1b,d–f) is a Holocene freshwater lake that formed approximately 8000 years ago and is located in between the two lagoons. At TKL, the sediments were coarse with pebbles at the bottom of the core (core length: 31.5 m) and became finer grained towards the top. Below 29.15 m measured from sediment surface, the sediments were frozen. The upper part of the TKL core consisted of unfrozen silty talik sediments. The core contained sediments with fresh pore water from top to bottom (EC_{max}: 1.3 mS/cm) [52].

The Polar Fox Lagoon (LAG1) (71.743056° N, 129.337778° E; Figure 1b,g,h), a nearly closed lagoon located in a partially drained lake basin, is connected to Tiksi Bay by an approximately

800-m-long and 50-m-wide channel. The channel stays frozen for about 8 months of the year, resulting in the seasonal isolation of the lagoon from Tiksi Bay and thus increasing liquid water salinity beneath the ice cover during the freezing season [25, 53]. At LAG1, the gray to dark gray sediments gradually became finer upwards in the core with shell and plant remains in the uppermost layers [19]. The upper part of LAG1 core (above 4.8 m) was saline and unfrozen [19].

Uomullyakh Lagoon (LAG2) (71.730833° N, 129.2725° E; Figure 1b,i,j), a shallow semi-open lagoon, is well connected to Tiksi Bay via a narrow opening in the center of a flat sand spit. Similar to LAG1, this connection allows for warm freshwater discharge from the Lena River into the lagoon in summer months, leading to significant seasonal and interannual variations in temperature and salinity. However, at LAG2, storm surges can also flood the sand spit that further influences the lagoon's hydrodynamics. Perhaps the most significant difference between LAG1 and LAG2 is the water depth. In winter, LAG2 is ubiquitously covered by bedfast ice, resulting in a direct atmosphere-sediment thermal coupling. Thermistor data showed cold sub-zero ($< -3°C$) sediment temperatures in the upper 30 m in April 2017. At LAG1, approximately 25% of the lagoon still contained floating ice by the end of the winter (in 2017), resulting in a hypersaline and cryotic pool of liquid water beneath the ice cover. Thus, while the sediment temperatures beneath the center of LAG1 are cryotic, they are significantly warmer than the center of LAG2 [19]. The surface sediment of the LAG2 core was characterized as silty fine sand [19]. The LAG2 core revealed a complex structure with alternating frozen and thawed sections during field analysis. Temperature reconstructions described in Jenrich et al. [19] revealed that the top 1 m of sediment was frozen because of bedfast ice. The core was saline from bottom to top [19].

3 | Methods

3.1 | Fieldwork and Subsampling

The sample material was retrieved on the Bykovsky Peninsula, Siberia, during two German-Russian field expeditions focusing on carbon and nitrogen stocks [19, 54, 55], OM source and quality [52], methane dynamics [25], microbiology [24], and the geophysical nature [53, 56–60] of the thermokarst affected peninsula and the nearshore subsea permafrost.

The permafrost outcrop TPF shown in Figure 1 was sampled during a field campaign in August 2014. Cylindrical samples (5 cm by 9 cm) in 3 replicates were drilled horizontally at seven depths with a hand-held electrical drill (Metabo, with HSS bimetal hole saw) into Yedoma deposits, ancient thermokarst deposits, and the active layer soil. The sediment cores were stored in pre-combusted glass jars and transported in a frozen state to AWI Potsdam. The sample below the organic layer was chosen for the incubation (see Figure 1c and Table 2).

The drilling of TKL, LAG1, and LAG2 took place during a field campaign to the Bykovsky Peninsula in April of 2017 [61]. Detailed descriptions of sub-aquatic permafrost evolution, core retrieval, and sectioning were given by Jongejans et al.

[52], Angelopoulos et al. [53], and Jenrich et al. [19] for TKL, LAG1, and LAG2, respectively. Briefly, sediment cores were taken from the center of the water bodies in TKL (core length: 31.5 m), LAG1 (core length: 27.7 m), and LAG2 (core length: 32.3 m) using a URB2-4T drilling rig (produced in Ozersk, Russia) mounted on a tracked vehicle, then sectioned and photographed. The cryolithology was described visually. The core sections were packed in core foil and transported frozen to AWI Potsdam.

For the incubation experiments, subsamples were taken from the surface (3–10 cm) of the cores and the outcrop. The 4 samples were kept frozen in pre-combusted glass jars until the start of the incubation experiments. Subsamples for hydrochemistry and geochemical analyses from the same depth were stored in WhirlPacks and weighed while frozen.

3.2 | Laboratory Analyses

3.2.1 | Hydrochemistry

For pre-incubation hydrochemical analysis, the pore water was extracted from thawed samples using Rhizon samplers (membrane pore size: 0.12–0.18 μm). Electrical conductivity (mS/cm), pH, dissolved organic carbon (DOC), and sulfate concentration were measured in the pore water.

To convert the measured electrical conductivity (referenced to 25°C) to molality (mol/kg) and absolute salinity (g/kg), we used the MATLAB implementation of TEOS-10 [62]. This conversion package assumes that the pore water fluid is consistent with standard seawater composition [63].

To be able to test the GHG production in different sediments during the phases of landscape development (lake, lagoon, and subsea), it is crucial to keep the seawater boundary conditions (fresh: c = 0 g/L, brackish: c = 13 g/L, marine: c = 36 g/L) and the total water volume of 10.5-mL constant. For this purpose, we have calculated, based on the molarity of the pore water, how much of the highly concentrated artificial seawater solution (c = 182.55 g/L) needed to be added to the samples. The artificial seawater solution had a concentration higher than that of standard seawater, so a relatively lower volume of water could be added to the sediment pore water and be diluted. In terms of the relative proportions of its components, the artificial seawater contained NaCl (24.99 g/L), $MgCl_2 \times 6H_2O$ (4.14 g/L), Na_2SO_4 (0.79 g/L), $CaCl_2 \times 2H_2O$ (1.58 g/L), KCl (11.13 g/L), and $NaHCO_3$ (0.17 g/L) dissolved in ultrapure water and sterile filtered after.

The pH and EC values were determined using a WTW Multilab 540 instrument, with an accuracy of ±0.01 for pH and ±1 mV for EC measurements. The DOC samples were treated with 50 μL of 30% HCl supra-pure, then stored at +4°C until analyzed using a Shimadzu Total Organic Carbon Analyzer (TOC-VCPH) with an accuracy of ±1.5%, following the method outlined by Fritz et al. [64].

Samples for measuring sulfate concentration were diluted (1:50) and subsequently analyzed in triplicates using the ion

chromatograph Sykam S155 Compact IC-System with a detection limit of 0.1 mg/L. Integration of measured peaks in the chromatograms was done automatically by the ChromStar 7 software. The average of the triplicated was used for further evaluation.

3.2.2 | Sedimentological and Biogeochemical Bulk Analyses

The sediment was weighed before and after freeze-drying (Zirbus Sublimator 15), and the absolute water content was determined based on weight difference between wet and dry sediment.

The samples for grain size analysis were treated with 35% H_2O_2 for 4–6 weeks to remove organic material. Subsequently, they were measured using a Malvern 316 Mastersizer 3000 with an attached Malvern Hydro LV wet-sample dispersion unit. The proportions of sand, silt, and clay fractions are provided as sums between 2 mm and 63 μm, 63 μm and 2 μm, and < 2 μm, respectively. Grain-size parameters were calculated with the software Gradistat (Version 8.0; [65]).

Homogenized and milled bulk samples (using a planetary mill Fritsch Pulverisette 5) were analyzed for total carbon (TC) and total organic carbon (TOC) content (expressed in weight percent [wt%]) using a soliTOC cube, as well as the total nitrogen (TN) content using a rapid max N exceed (both Elementar Analysensysteme, Langenselbold, Germany; both with a device-specific accuracy of ± 0.1 wt% and a detection limit of 0.1 wt%).

On a separate aliquot for stable carbon isotope analysis (δ¹³C-TOC), carbonates were removed from sediments with 1.3-M hydrochloric acid (HCl) at 50°C for 5 h. Afterwards, chloride ions were washed out of the samples, and the samples were dried again. Stable carbon and nitrogen isotopes (δ¹⁵N-TN) were then measured at AWI ISOLAB Facility Potsdam using a ThermoFisher Scientific Delta-V-Advantage gas mass spectrometer equipped with a FLASH 2000 elemental analyzer EA and a CONFLO IV with a accuracy of ±0.01‰.

3.2.3 | Incubation Experiment Set Up

To simulate the GHG production during the stages of coastal permafrost landscape development (lake formation–lagoon formation–subsea) under laboratory conditions (Table 1), we developed a systematic approach (Figure 2). We used TPF sediment from an outcrop close to the coast and incubated it with (1) sterilized tap water (fresh water conditions) to simulate a freshly formed lake, (2) with artificial brackish water to simulate a freshly formed lagoon, and (3) with artificial seawater to simulate subsea conditions after sea water inundation. Also, we incubated surface talik sediment of a thermokarst lake under the same three conditions. By maintaining freshwater conditions, we investigate the GHG production in an established lake. The incubation of the lake sediment under brackish conditions simulates a young lagoon, while incubating under marine conditions simulates either a highly saline lagoon or recently submerged sediment beneath the sea. The lagoon sediments contained salts initially, so we omitted simulating the freshwater state. We used sediments from the two lagoons because they differ in age and connectivity with the sea and therefore represent two states of lagoon genesis. The younger and more isolated nearly closed lagoon (LAG1) can be considered as an established lagoon, while the older more open LAG2 lagoon represents an old lagoon. Incubating the lagoon sediments under brackish conditions represents their mean annual salinity state because the incubated samples were close to the water/sediment interface. The mean annual salinity for Tiksi Bay is known to be brackish based on measurements of bottom water temperature and conductivity over the course of an entire year [66]. By incubating the lagoon sediments with marine water, the subsea stage is represented. We acknowledge that submerged sediments close to the coast of the Bykovsky Peninsula still experience brackish conditions, but for simplicity, we ignore the effects of river discharge for the subsea stage. In the further course, we use the term near natural conditions for the incubation conditions that are most similar to in situ conditions. In the case of permafrost and lake sediments, we use to near natural conditions when we refer to freshwater conditions, whereas for lagoon sediments, near natural conditions are brackish conditions.

Given the well-established anaerobic conditions in waterlogged soils in situ, we conducted the incubation anaerobically.

TABLE 1 | Applying the laboratory incubation approach to the landscape level.

	Incubation condition		
Sediment	**Freshwater**	**Brackish**	**Marine**
TPF	Young thermokarst lake[a] (low OM decomposition)	Young lagoon (low OM decomposition)	Young subsea (low OM decomposition)
TKL	Old thermokarst lake[a] (high OM decomposition)	Young lagoon (high OM decomposition)	High-saline lagoon or young subsea (high OM decomposition)
LAG1	—	Established lagoon[a] (medium OM decomposition)	Subsea (medium OM decomposition)
LAG2	—	Old lagoon[a] (high OM decomposition)	Subsea (high OM decomposition)

Note: Incubation conditions: anaerobic, 4°C, 1 year, freshwater (0 g/L), brackish (13 g/L), brackish (36 g/L).
Abbreviations: LAG1 and LAG2, saline surface lagoon sediments of different age; TKL, thermokarst lake talik sediment; TPF, terrestrial permafrost sediment.
[a]Considered as near-natural conditions.

Sampling

Processing

Pre-analysis

Incubation

1 year at 4°C, anaerobic, dark

CO_2 and CH_4 measurements
(250-µL subsample)
- first 2 weeks: 5 times
- following 8 weeks: once a week
- after that: biweekly

Measuring device:
Gas Chromatograph
Agilent GC 7890A with an
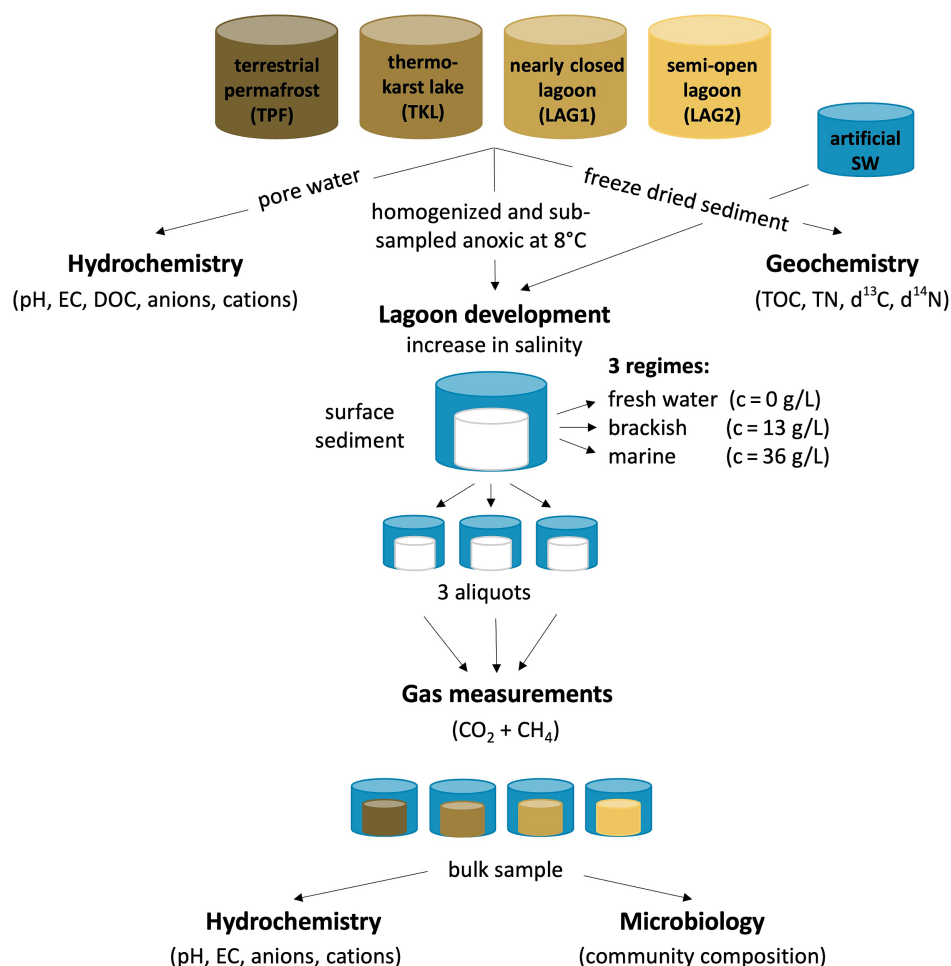Agilent HP-PLOT Q column

Processing

Post-analysis

FIGURE 2 | Design of the incubation experiment displaying the steps from sampling to post-analysis. In total, 36 incubation vials (4 locations, 3 salinity treatments and 3 aliquots for each approach) were analyzed. Scheme modified after Tanski et al. [28]. [Colour figure can be viewed at wileyonlinelibrary.com]

To be able to test the GHG production in different sediments during the phases of landscape development (lake, lagoon, subsea), it is crucial to keep the seawater boundary conditions (fresh: c = 0 g/L, brackish: c = 13 g/L, marine: c = 36 g/L), the total water volume of 10.5 mL, and the amount of soil (5 g of dry weight) constant. For this purpose, we have calculated, based on the molarity of the pore water, how much of the highly concentrated artificial seawater solution (c = 182.55 g/L) needed to be added to the samples. The artificial seawater solution had a concentration higher than that of standard seawater, so a relatively lower volume of water could be added to the sediment pore water and be diluted. In terms of the relative proportions of its components, the artificial seawater contained NaCl (24.99 g/L), $MgCl_2 \times 6H_2O$ (4.14 g/L), Na_2SO_4 (0.79 g/L), $CaCl_2 \times 2H_2O$ (1.58 g/L), KCl (11.13 g/L), and $NaHCO_3$ (0.17 g/L) dissolved in ultrapure water and sterile filtered after. Depending on the initial pore water content and salinity, different amounts of wet soil had to be weighed in and different volumes of artificial seawater added for the samples respectively to the treatment. More detail is given in Table S1.

To ensure the exclusion of oxygen, which could adversely affect anaerobic microbial communities, we discarded the upper 3 cm of the sediment sample (given a maximum oxygen penetration depth of 25 mm [67]) and maintained an oxygen-free atmosphere during sample preparation (overnight thawing and handling under a pure nitrogen atmosphere in a glovebox at 8°C) and the incubation. In the glovebox, we homogenized the samples and filled them into pre-combusted 120-mL glass incubation vials. Three replicates were prepared for each treatment. Before starting the experiment, the headspace was flushed with pure nitrogen for 2 min. The oxygen concentration in the headspace of a test vial was measured at the beginning and regularly within the first 3 months of the experiment, remaining below 0.012%. The incubation temperature was set at 4°C, approximately corresponding to the temperature of the water at the bottom of the water bodies in summer, and for comparability with other permafrost incubation studies (e.g., [28, 31]).

Concentrations of CO_2 and CH_4 were measured by gas chromatography (7890A Agilent, United States) equipped with a thermal conductivity detector and a flame ionization detector to measure CO_2 and CH_4 concentrations, respectively, with helium as the carrier gas and the oven furnace temperature of 100°C. Before each measurement, the incubation vials were shaken to avoid zonation in sediment and water. Gas samples were drawn from the headspace of the vials with a gastight syringe and then immediately injected into the gas

chromatograph. We carried out the measurements 5 times during the first 2 weeks, weekly for the following 8 weeks, and bimonthly thereafter. The amount of gas produced was calculated in parts per million (ppm) and normalized to sediment's dry weight (gdw^{-1}). Using the gas concentration, headspace volume, water volume, pH, temperature, and solubility—including carbonate and bicarbonate concentrations for CO_2 calculations [68]—the total amount of CO_2 and CH_4 was determined in µmol using the ideal gas law [37]. By employing the molar mass (M) of C (12), the obtained amount of CO_2 and CH_4 in µmol was normalized to gdw^{-1} and recalculated into mg CO_2-C gdw^{-1} and CH_4-C gdw^{-1}. We further calculated the average for CO_2 and CH_4 production for the three replicates and normalized the results to gSOC^{-1} using the TOC content. A detailed method description including calculation formulas can be found in Section S1.2.

3.3 | Microbiology Analyses

3.3.1 | DNA Extraction, PCR, and Sequencing

Total nucleic acids were extracted in duplicates using the PowerSoil-Kit (MO-Bio) according to the manufacturer's protocol. Amplicon libraries were prepared by using barcoded primer pair sets (Uni515-F[5′-GTGTGYCAGCMGCCGCGGTAA-3′]/Uni806-R[5′-CCGGACTACNVGGGTWTCTAAT-3′]), with duplicates for each sample. PCR reactions (50 µL) contained 10× Pol Buffer C (Roboklon GmbH, Berlin, Germany), 25-mM MgCl$_2$, 0.2-mM dNTP mix (ThermoFisher Scientific), 0.5-mM each primer (TIB Molbiol, Berlin, Germany), and 1.25 U of Opti Taq Polymerase (Roboklon, Germany). The PCR program included an initial denaturation step at 95°C for 7 min, followed by 33 cycles at 95°C for 15 s, annealing at 60°C for 30 s, extension at 72°C for 30 s, and a final extension step at 72°C for 5 min. After purification with the Agencourt AMPure XP kit (Beckman Coulter, Switzerland), the recovered PCR products were equilibrated into comparable equal amounts before pooling with positive and negative controls. For the positive controls, we utilized a commercially available mock community (ZymoBIOMICS Microbial Community DNA Standard II). As for the negative controls, they consisted of the DNA extraction buffer and the PCR buffer. Sequencing was run in paired-end mode (2 × 300 bp) on Illumina MiSeq platform by Eurofins Scientific (Konstanz, Germany).

3.4 | Data Analyses

3.4.1 | Microbiology

The raw data were processed by an in-house pipeline. Briefly, the demultiplexing was performed using cutadapt [69]. The resulting sequences were further processed in DADA2, including steps of filtering, dereplication, chimera detection, sequence merging, and the identification of amplicon sequence variants (ASVs) [70]. The taxonomy was assigned against the SILVA138 database [71]. The clustering dendrogram was generated on the Bray–Curtis dissimilarity using the "hclust" function from the base package "stats" embedded in R (v4.3.0) (R Core Team). The Bray-Curstis dissimilarity was calculated

by using the "vegdist" function from the R package vegan (v2.6-4) [72]. The bubble plot at the taxonomic rank family was generated by the ggplot2 package (v3.4.2) [73]. The community data were collapsed at family level by package otuSummary (v0.1.1) [74].

3.4.2 | Calculating Response Ratios

For investigating how GHG production changes depending on salinity increase, we calculated response ratios by dividing the mean cumulative production per gram C for terrestrial sites (TPF and TKL) under freshwater conditions by that under brackish conditions (B$_{terr}$:F$_{terr}$), respectively with brackish and marine for the lagoons LAG 1 and LAG2 (M$_{lag}$:B$_{lag}$). Even though the sediment was homogenized before preparing the bottles and the replicates were treated equally, the GHG production differed. Therefore, we divided the value of each replicate of F and B by each replicate of B and M respectively. The data ($n = 18$) was visualized as boxplots in Microsoft Excel Version 16.8.

4 | Results

4.1 | Environmental Parameters

The results of the environmental parameters show distinct patterns in various parameters across the studied locations, as displayed in Table 2, providing insights into the environmental conditions and sediment characteristics.

We found that the TPF outcrop shows consistently high values for DOC (158.70 mg/L), TOC (9.06 wt%), and TN (0.54 wt%) and the highest depletion of δ^{13}C (−28.85‰).

Conversely, LAG2 stands out with the lowest values for most parameters, including DOC (41.32 mg/L), TOC (2.03%), TN (0.14%), and a higher δ^{13}C value (26.6‰). These findings suggest lower carbon and nitrogen content in the sediment and the pore water of LAG2, indicative of a potentially different environmental and depositional history. Remarkably, the DOC concentration at LAG1 is 3 times higher compared to LAG2.

Highest mean grain size was found at LAG2 (16.1 µm). This is attributed to the lagoon's openness, allowing the input of sandy marine depositions. Contrastingly, LAG1 exhibits the lowest mean grain size (5.9 µm), characterized by fine-grained lake deposits. There is low or no input of sandy marine sediment due to the long inlet channel.

The TKL stands out with the highest ice/water content (58.53%). In contrast, LAG2 exhibits the lowest ice/water content at 47.14%, suggesting a lower presence of frozen water in its sediment caused by the lower pore volume reflecting the coarser grain size in LAG2.

Hydrochemical measurements show that LAG1 had the highest pH (7.67) and EC (40.5 mS/cm) values, indicating alkaline and saline conditions. This is in stark contrast to TPF outcrop, which exhibits the lowest pH (5.12). The nearly closed

TABLE 2 | Overview of the environmental parameters of the surface sample at the four study sites.

Site	System	Name	Sample depth (cm)	Thermal state	Grain size description	Mean grain size (µm)	Ice/water content (%)	pH	EC (mS/cm)	Salinity (g/L)	Sulfate (mg/L)	DOC (mg/L)	TOC (wt%)	TN (wt%)	TOC/ TN	d¹³C (‰)
1	TPF	Terrestrial permafrost	Byk14 outcrop	30–35	Active layer	Very poorly sorted medium silt	11.17	52.49	5.12	0.2	0.1	<0.1	158.70	9.06	0.54	16.87	−28.9
2	TKL	Thermo-karst lake	Goltsovoye Lake	5–17	Talik	Very poorly sorted fine silt	7.48	58.53	5.93	0.2	0.1	<0.1	NA	4.03	0.31	13.21	−28.6
3a	LAG1	Nearly closed lagoon	Polar Fox Lagoon	3–10	Talik	Poorly sorted fine silt	5.90	51.34	7.67	40.5	26.1	75.84	126.20	4.03	0.26	15.38	−27.5
3b	LAG2	Semi-open lagoon	Uomullyakh Lagoon	3–10	Seasonally frozen	Poorly sorted coarse silt	16.09	47.14	7.01	35.4	22.4	319.41	41.32	2.03	0.14	14.58	−26.6

Abbreviations: d¹³C: stable carbon isotope composition of TOC; DOC: dissolved organic carbon; EC: pore water conductivity; Salinity: salinity of the pore water; Sulfate: sulfate concentration; TN: total nitrogen; TOC: total organic carbon; TOC/TN: carbon-nitrogen ratio.

nature of Polar Fox Lagoon contributes to high salinity particularly due to brine formation below the lagoon ice in winter. Although LAG2 is shallower and hypersaline throughout many parts of its core, its total surface sediment salinity is similar to LAG1.

The terrestrial sites showed a similarly low electrical conductivity (0.2 mS/cm).

Sulfate concentrations at LAG2 were four times higher than those at LAG1, indicating a greater influence of the sea at LAG2. This can probably be mainly attributed by its closer proximity, but also by the shallow depth of LAG2. Hypersaline water beneath the lagoon ice cover can elevate sediment salinity [19]. Although this is not apparent in the total salinity of the surface sample (representing all dissolved ions), hypersaline conditions are consistently observed throughout the LAG2 core over a 30 m depth range [19]. As expected, there were no detectable sulfate concentrations at terrestrial freshwater sites (detection limit SO_4^{2-}: 0.1 mg/L).

The TPF outcrop exhibits the highest TOC/TN ratio (16.87). Conversely, TKL displays the lowest TOC/TN ratio (13.21).

4.2 | Microbial Community Composition

The relative abundance analysis of archaea and bacteria shown in Figure 3 revealed that lagoons exhibited the highest microbial diversity, followed by the lake, while permafrost displayed the least diversity. The Bray–Curtis dissimilarity analysis (Figure 4) revealed that microbial communities tended to cluster based on landform. Lagoons notably formed a distinct cluster, and a larger group encompassed all inundated sites. In contrast, permafrost stood out as markedly different from other sites. Furthermore, the local signature of the microbial communities remained also at the end of the incubations.

The most substantial shift in microbial composition over the one-year incubation period was observed for the permafrost. The microbial community was dominated initially by Pseudomonadaceae, known for aerobic chemoorganotrophic respiratory metabolism, and shifted towards anaerobic microorganisms during the incubation (Figure 3). In contrast, there was much less change observed for the lagoons.

A specific difference is that lineages that are able to reduce sulfate (Desulphobacteria) occur to a greater extent in the lagoon sediments than in the non-lagoon sediments.

Methanogenic Archaea were abundant in permafrost sediments before the incubation (initial) and after the incubation, with highest relative abundance under freshwater conditions. Their relative abundance decreased with increasing salinity. In the lake and the lagoons, their presence was either minimal (< 0.5%) or not detectable, but after 1 year of incubation, there was an increase in LAG1, correlating with substantial methane production in LAG1.

Clostridiaceae and Acidobacteriota are thriving in permafrost and lake environments (Figure 3). In lagoons,
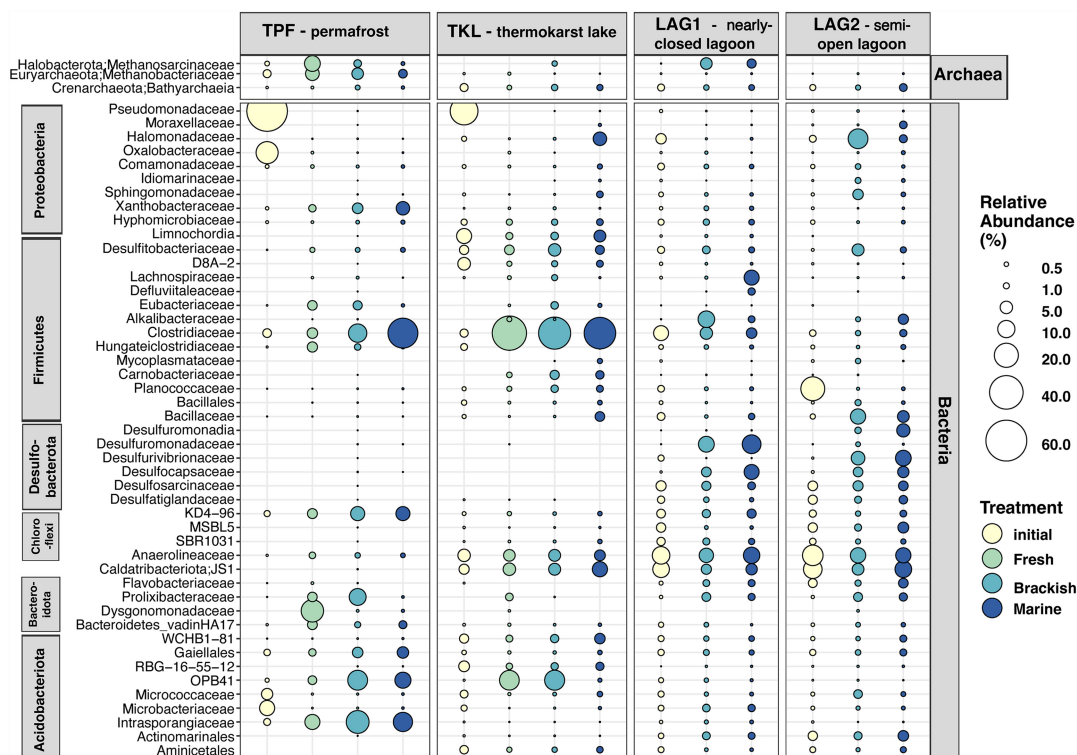
FIGURE 3 | Bubble plot showing the relative abundance of archaea and bacteria before the incubation (initial, yellow) and after the incubation with freshwater (green), brackish water (turquoise), and marine water (blue) for the four study sites (TPF [permafrost outcrop], TKL [Goltsovoye Lake], LAG1 [Polar Fox Lagoon], and LAG2 [Uomullyakh Lagoon]). The bubble size denotes the relative abundance of different taxa. Bubbles decreasing in size from before to after incubation indicate that the treatment has a negative effect on the microorganisms present, while bubbles increasing in size indicate favorable conditions. The taxonomy was collapsed at family level. If an assignment to the family level was not possible the next higher assignable taxonomic level was used. [Colour figure can be viewed at wileyonlinelibrary.com]
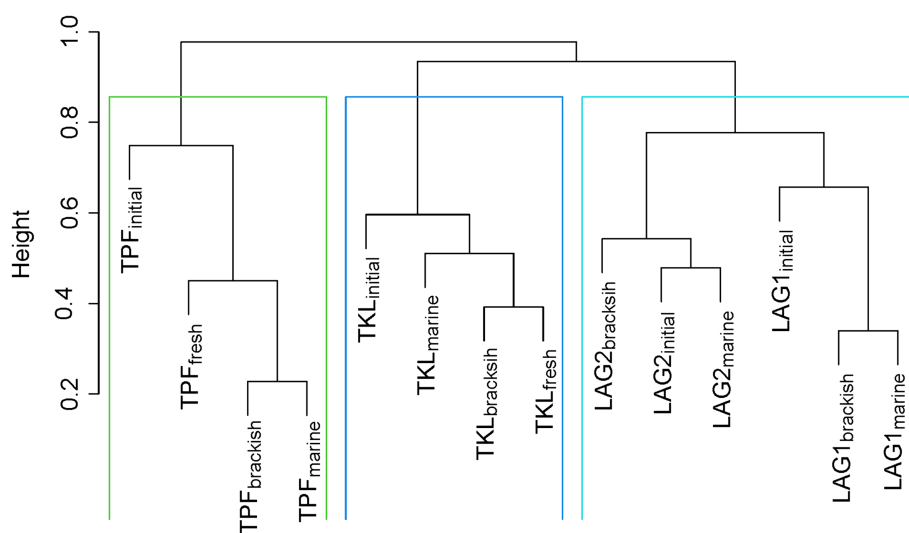

FIGURE 4 | Clustering dendrogram based on Bray–Curtis dissimilarity shows that microbial communities group by landform (TPF [permafrost outcrop], TKL [Goltsovoye Lake], LAG1 [Polar Fox Lagoon], and LAG2 [Uomullyakh Lagoon]) rather than treatment (fresh [no addition of artificial seawater], brackish c = 13 g/L, marine c = 36 g/L). [Colour figure can be viewed at wileyonlinelibrary.com]

Desulfuromonodaceae, anaerobic sulfur reducers, dominated. Sulfur and sulfate reducers had already established in the lagoons and remained abundant in the salinity treatments, whereas in permafrost and the freshwater lake, they did not occur initially and also not at the end of the incubation. This coincided with the stronger development of CO_2 in the saline sites compared to the freshwater sites. Halomonadaceae were dominant in lagoon LAG2, especially under brackish conditions.

4.3 | Cumulative Anaerobic CO_2 and CH_4 Production

The results on the cumulative anaerobic CO_2 and CH_4 production measured after 363 days are shown in Figure 5. The CO_2 production ranged from 0.001 ± 0 mg CO_2-C gdw^{-1} for TKL-F to 0.91 ± 0.03 mg CO_2-C gdw^{-1} for LAG1-B (Figure 5a). When normalized to soil organic carbon (SOC) content, both lagoons exhibited similar patterns in CO_2 production under brackish and marine conditions (22.7 ± 0.8 and 22.1 ± 3.1 mg CO_2-C gSOC^{-1} for LAG1 and LAG2, respectively) (Figure 5b). At each location the highest CO_2 production occurred under near-natural conditions (freshwater for TPF and lake, brackish for lagoons). The CO_2 production decreases with increasing salinity under the laboratory conditions.

The methane production ranged from 5.4×10^{-6} mg CH_4-C gdw^{-1} for LAG2-M to 0.53 mg CH_4-C gdw^{-1} for TPF-F (Figure 5c); therefore, methane production per gram of dry weight was highest in the permafrost sample incubated with freshwater (young lake). When normalized to SOC, LAG1 under brackish conditions exhibited higher CH_4 production (7.24 ± 0.3 mg CH_4-C gSOC^{-1}) compared to the permafrost sample (TPF-F) (5.85 ± 0.2 mg CH_4-C gSOC^{-1}). In contrast to LAG1-B, no methane was produced in LAG2 (Figure 5d).

The thermokarst lake displayed the lowest CO_2 and CH_4 production overall (< 0.003 mg gdw^{-1}).

The contribution of CO_2 to cumulative GHG production after 362 days ranged from 40.1% at TKL-F to 99.9% at LAG2-B and

LAG2-M (Figure 5e). There was equal CO_2 and CH_4 production for TPF under freshwater conditions. For brackish and marine conditions, CO_2 production dominated, with a share greater than 75.8%.

During the 1-year incubation period, we observed shifts in CO_2 and CH_4 headspace concentrations. In several samples (Figures S1a [TPF-B and TPF-M], S1e [TKL-F and TKL-B], and S2a [LAG1-B and LAG1-M]), we noted a sharp increase in headspace CO_2 concentration in the initial weeks of the incubation, followed by a rapid decline within the first weeks.

Further, for LAG1-B, we observed an exponential increase in both cumulative CH_4 production and daily CH_4 production rates from day 100 until approximately day 220 (Figure S2b,d). After this period, daily rates of CH_4 production dropped, coupled with a stagnation in cumulative CH_4 production.

By calculating the response ratios, we found that if TPF or talik sediment comes in contact with sea water (scenario $F_{terr} \rightarrow B_{terr}$ in Figure 6a,b), less CO_2 and CH_4 was produced in the incubation period. The decrease in methane production is slightly higher from fresh to brackish (median 0.12) than from brackish to marine conditions (median 0.16). However, the ratio of the cumulative CO_2 production for terrestrial samples versus lagoon samples under near-natural conditions ($F_{terr} \rightarrow B_{lag}$ in Figure 6c) is greater 1 (median: 326.9), showing that CO_2 production increases significantly in the long-term, after lagoon formation. CH_4 production on the other hand decreases in the long term (median: 0.6).
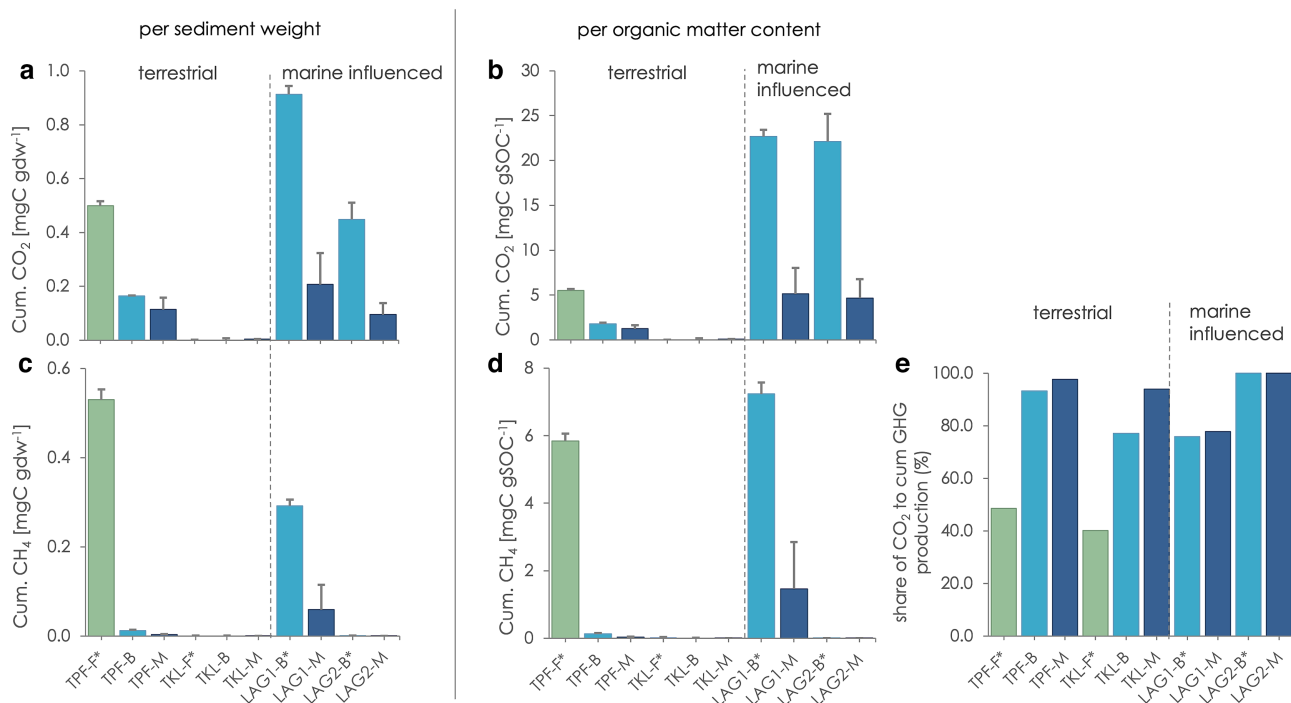

FIGURE 5 | Cumulative anaerobic CO_2 and CH_4 production over the 363-day incubation at 4°C for freshwater (green), brackish (turquoise) and marine (dark blue) conditions. (a) cumulative CO_2 production in mg per gdw; (b) cumulative CO_2 production in mg per gSOC; (c) cumulative CH_4 production in mg per gdw; (d) cumulative CH_4 production in mg per gSOC; (e) percentage share of CO_2 to cumulative GHG production, the difference to 100% is equivalent to the share of CH_4. TPF: terrestrial permafrost outcrop TPF; TKL: thermokarst lake Goltsovoye; LAG1: nearly closed Polar Fox Lagoon; LAG2: semi-open Uomullyakh Lagoon; *near-natural conditions. [Colour figure can be viewed at wileyonlinelibrary.com]
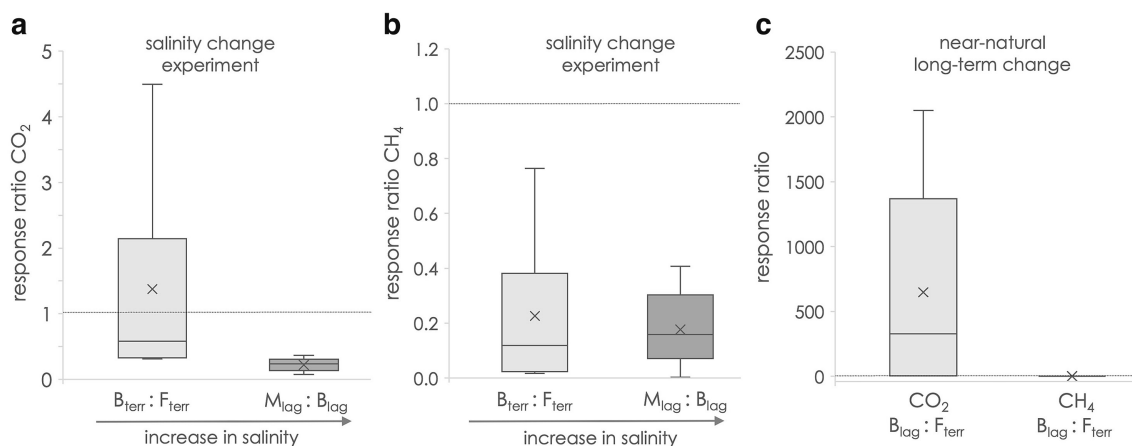
FIGURE 6 | Ratio of cumulative (a) CO_2 and (b) CH_4 production per gram SOC from fresh to brackish conditions at the terrestrial sites (B_{terr}:F_{terr}) and from brackish to marine conditions for the lagoons (M_{lag}:B_{lag}). (c) Ratio of cumulative CO_2 and CH_4 production per gram SOC for terrestrial samples versus lagoon samples under near-natural conditions (B_{lag}:F_{terr}). Response ratio < 1 indicates a decrease in production, response ratio = 1 indicates no change and response ratio > 1 indicates increasing production. Box-whisker plots with outliers outside the lower and upper quartiles. Mean is symbolized by x.
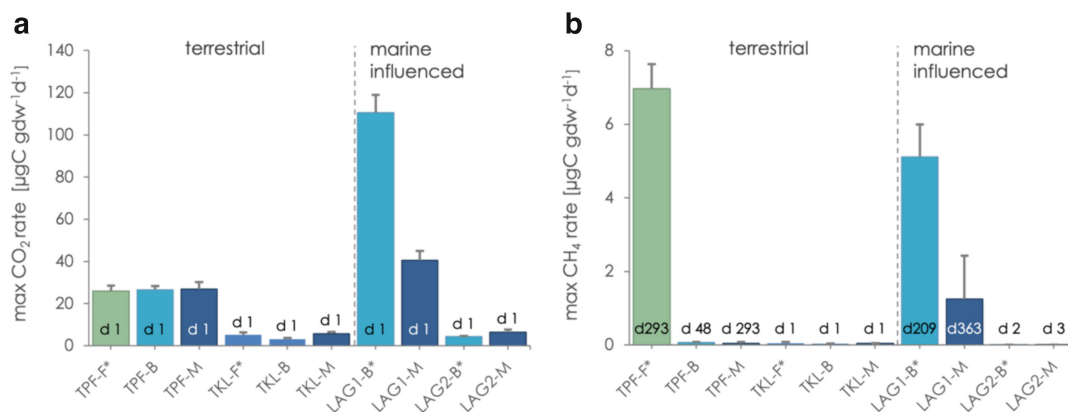

FIGURE 7 | (a) Maximum CO_2 production rates in µg gdw^{-1} d^{-1} and (b) maximum CH_4 production rates in µg per gdw^{-1} d^{-1} for freshwater (green), brackish (turquoise), and marine (dark blue) conditions. The day of the maximum production rate is labeled at the base of the bars. TPF: terrestrial permafrost outcrop TPF; TKL: thermokarst lake Goltsovoye; LAG1: nearly-closed Polar Fox Lagoon; LAG2: semi-open Uomullyakh Lagoon; *near-natural conditions. [Colour figure can be viewed at wileyonlinelibrary.com]

4.3.1 | Production Rates

Median CO_2 production rates ranged from 0.2 to 77.6 µg CO_2-C gSOC^{-1} d^{-1}. Maximum CO_2 production rates were measured on the first day for all samples and ranged between 3.1 µg CO_2-C gdw^{-1} d^{-1} and 110.4 µg CO_2-C gdw^{-1} d^{-1} for TKL-B and LAG1, respectively (Figure 7a).

Median CH_4 production rates ranged from 0.001 to 4.4 µg CH_4-C gSOC^{-1} d^{-1} and the maximum CH_4 production rates ranged between 0.002 µg CH_4-C gdw^{-1} d^{-1} for LAG2-M and 6.96 µg CH_4-C gdw^{-1} d^{-1} for TPF-F (Figure 7b). For those samples with neglectable CH_4 production (TKL and LAG2), the highest production rate was measured in the first days of incubation while for the others the maximum production rate was measured towards the end of the incubation period.

5 | Discussion

5.1 | Local Short-Term Response to Different Incubation Settings

5.1.1 | Microbial Composition and Response to Changing Salinity

Microbial communities cluster based on landform, especially for lagoons, which show a unique cluster (Figure 4). In detail, a larger group encompassed all inundated sites, while TPF stood out. It shows that microbial composition is highly shaped by the initial environmental conditions, with microbes in TPF being aerobic, in contrast to inundated sites, in which many are anaerobic. Additionally, there is an absence of sulfate for TPF and lake, whereas sulfate is present for the lagoons. Furthermore,

the local signature of the microbial communities was still observed at the end of the incubations, suggesting that the time of incubation was too short for convergence of the communities according to treatments.

In our incubation experiment, a combination of stress factors likely caused the TPF to experience the most substantial shift in microbial composition between before the incubations (ice-bonded permafrost) and after the incubations (inundated). The shift from the dominating Pseudomonadaceae, known for aerobic chemoorganotrophic respiratory metabolism, towards a variety of anaerobic microorganisms (Figure 3), suggests that the lack of oxygen had a major impact on the microbial composition. Further, the abrupt thawing and the phase transition from ice to liquid water is one of the major stress factors for the biological system [75] and leads to rapid changes in the structure of the permafrost microbiome [76–79]. There is also a difference in microbial composition between freshwater and brackish/marine incubations of the permafrost (TPF in Figure 3) but it is less pronounced, indicating that the changing salinity has a smaller impact than the thermal state and the availability of oxygen. Nevertheless, microbes have a salinity optimum for growth and a rapid shift in salinity might cause lower activity [80, 81].

In contrast to the drastic microbial composition changes in the TPF following changing conditions, less changes were observed in the lake and the lagoon sample incubations, suggesting that the initial microbial communities were already adapted to thawed and inundated conditions. However, the microbial community in the lake differs considerably from that in the lagoons. Even after 1 year of incubating with sulfate-containing seawater, the proportion of SRB did not increase (Figure 3), indicating that the initial microbial community did not adapt to marine conditions in the short term and under the conditions of a closed system. In the permafrost and lake samples, the presence of spore-forming Clostridia suggests a response to disturbance, while the ability of Acidobacteria utilizing stable carbon sources proved advantageous at low substrate concentrations. New studies showed that some Acidobacteria, including OPB41, which were thriving in the terrestrial samples, use sulfate as electron acceptors [82], and some Acidobacteria are able to switch between dissimilatory sulfate reduction and oxygen respiration [83], streamlining the multi-step mineralization of complex organic substances into CO_2 into a single process. The flexibility and adaptability of the Acidobacteria make them particularly successful in the terrestrial samples, where Desulfobacteriota (SRB) could not develop during the incubation time.

Recent research at the same study sites as ours by Yang et al. [24] explored how variations in geochemistry influenced the microbial methane-cycling community in two thermokarst lakes (Goltsovoye Lake, TKL and Northern Polar Fox Lake) and Polar Fox Lagoon. They observed that non-competitive methylotrophic methanogens dominated the methanogenic communities in both lakes and the lagoon, leading to elevated CH_4 concentrations in sulfate-poor sediments. In the nearly closed Polar Fox Lagoon (LAG1), we found that the abundance of both, Methanosarcinaceae and SRB, increased during the incubation, demonstrating that even in the presence of sulfate and SRB methanogens may grow. The co-habitation of methanogens

and sulfate reducers in marine environments was also noticed by other studies [24, 84–86]. We found that microbial communities were most diverse at brackish conditions, confirming previous findings showing that lagoons are unique microbial habitats [24].

Apart from this, the microbial composition in the lagoon samples remained similar before and after incubation, indicating that the microbial community was already adapted to saline conditions.

In contrast to nearly closed LAG1, the existence of methanogens is negligible at the more connected lagoon LAG2, which is likely due to the more distinct marine character pronounced by the four-time higher sulfate concentration. The adaptation to more sulfate-rich conditions is shown by the increase in SRB abundance with salinity.

5.1.2 | Potential C Production Response

5.1.2.1 | Variability in Carbon Dioxide Production. The elevated CO_2 production observed in near-natural conditions (freshwater for permafrost and lake, and brackish for the lagoons) compared to the lower levels in more saline treatments (Figure 5) suggests that the treatments induced disturbances rather than positive stimuli, which points towards a very strong microbial control. Even though electron acceptors in the form of sulfate were added to the permafrost and talik sample (TPF, TKL in Figure 2) in the brackish and marine treatment, CO_2 production did not increase, likely because of a lack of microbes (SRB) that can use them (Figure 7). Due to the closed system setting and the use of sterile artificial seawater, there was no external input of marine microbes and the existing community was not able to adapt to saline conditions in the incubation time.

Our median CO_2 production rates (0.2–77.6 µg CO_2-C gSOC^{-1} d^{-1}) were slightly higher but in general agreement with other anaerobic incubations (median: 1.6–50 µg CO_2-C gSOC^{-1} d^{-1}; [29, 31, 87]). Other studies found higher cumulative CO_2 production but different conditions prevailed (e.g., [28, 32, 88, 89]. Like other studies, we found a relationship with %C [29, 30], which is most pronounced in the CO_2 production in the lagoon sediments. When normalized to SOC, the same amount of CO_2 was produced in both lagoons (Figure 5b), suggesting the sediment origin plays a secondary role. Previous findings by Jenrich et al. [19] found that the surface sample at LAG2, low in TOC and TN, is very likely a mix of lacustrine and marine sediment, which was transported into the lagoon from the bay and therefore differs to the surface sediment of LAG1. The enclosed LAG1 on the other hand functions more as a sediment trap, capturing materials eroded from the Yedoma uplands and the shoreline, particularly OC-rich materials. LAG2 is more open and less of a trap so that OC can be exported into the ocean more easily. These sediment dynamics emphasize the importance of considering local variations in lagoon environments, especially when upscaling GHG production.

In the initial weeks of the incubation experiments, we observed a rapid decrease in headspace CO_2 concentration across several samples, regardless of the treatment (Figures S1a,e

Permafrost and Periglacial Processes, 2024

and S2a). Since this trend was consistent across all three replicates and the CH_4 concentration remained constant or increased, we can rule out the possibility of a leak. Similar patterns were observed in previous incubation experiments [31, 90, 91]. Bischoff [90] suggested that higher CO_2 solubility in water under high pressure led to a decrease in headspace CO_2 concentration. However, after the initial drop, the CO_2 concentration increased, surpassing the pre-drop levels in most samples. This suggests that the pressure increased as well and therefore cannot be the only reason for the declining concentration. Furthermore, we did not observe an extreme decline in pH during the incubations (Table S2), which would be expected for high CO_2 uptake in the water. Even for TKL, where CO_2 levels stayed low after the drop, the pH was higher at the end of the incubation.

Non-phototrophic CO_2 fixation, also known as dark CO_2 fixation, is a process by which soil bacteria can fix CO_2. Several soil types, including those found in Arctic tundra, have shown signs of this process [92, 93]. Using incubation experiments, they demonstrated that rates of dark CO_2 fixation increase with increasing headspace CO_2 concentrations [93–95]. Although dark CO_2 fixation is low compared with respiration rates, it might be a more plausible explanation for the observed decline in CO_2 concentration in our incubation experiments. Further research is needed to support this.

5.1.2.2 | Variability in Methane Production. In only two of our samples (TPF-F and LAG1-B), significant quantities of CH_4 were produced (Figure 5c). For these samples, the production rates correlated with the Archaea concentration (Figure 3). Furthermore, the start of CH_4 production was about 150 days after the incubations started (Figures S1b and S2b). Similar or even longer lag phases were reported by prior studies which concluded that the low initial colonization of methanogens caused the delay [29, 31, 37, 96, 97]. Median CH_4 production rates (0.001–4.4 µg CH_4-C gSOC^{-1} d^{-1}) were low but in the range of other anaerobic studies (0.02–135.1 µg CH_4-C gSOC^{-1} d^{-1}; [29, 31, 35, 87, 98]).

The permafrost sample incubated with freshwater (young lake; Table 1) exhibited the highest methane production per sediment weight, highlighting the considerable methane release potential in freshly formed thermokarst ponds and lakes. Studies indicated faster CH_4 production from younger carbon compared to older carbon based on 14C ages in DOC in northern lakes [36, 99, 100]. However, Walter Anthony et al. [101] demonstrated that CH_4 emitted as gas bubbles, the dominant pathway of methane emissions from northern lakes, is older than dissolved CH_4 in the water column. In this study, under near-natural conditions, LAG1 showed higher CH_4 production normalized to SOC compared to the permafrost sample (Figure 5d), indicating differences in OM degradability. Notably, we detected methane production for LAG1 under marine conditions after a lag phase of about 300 days (Figure S2b), likely due to the abundance of non-competitive methanogens. These findings are consistent with Yang et al. [24]. In contrast, no methane was produced in LAG2, possibly due to the absence of an initial methanogenic community (Figure 3) and the more disturbed environmental setting compared to LAG1. The UWITEC core of LAG1 [53] showed

a diffusive salinity profile, indicative of gentle surface conditions. The upper 5 m of sediment were identified as lacustrine [19]. In contrast, the surface sediment of LAG2 was characterized by a mix of lacustrine and marine deposits. Also, initial sulfate concentrations in LAG1 are lower than in LAG2, which may pave the way for both CO_2 and CH_4 production at the same time. This again fits very well to the findings of Yang et al. [24], who measured high methane concentrations in all sulfate-poor sediments. Further, the surface sediment of LAG2 freezes every winter due to the formation of bottom-fast ice opposed to LAG1 where the microbial community may persist year-round. In addition to the higher sulfate content, this significant microbial stressor may also be why LAG2 has a less established methanogenic community. Further, [102] found that in thawing permafrost sediments, CH_4 production is influenced most by paleoenvironmental conditions during soil formation. They also highlighted the vulnerability of CH_4 production due to its restriction to a small group of archaea, contrasting with the various microbial groups contributing to anoxic CO_2 production.

Moreover, it can be assumed that the oxidation of CH_4 to CO_2, known as anaerobic oxidation of methane (AOM), plays a role in our incubation experiment. In their study of the same sites, Yang et al. [24] demonstrated the presence of AOM-performing archaea in the sediments. In LAG1 (PFL in Yang et al.), marine anaerobic methanotrophic archaea (ANME-2a/2b groups) were identified, while in TKL (LG in Yang et al.), terrestrial AOMs were detected. The influence of AOM, visible in δ^{13}C-CH_4 signatures and gas concentrations, was only observed in LAG1, suggesting that AOM primarily occurs in marine environments. It is therefore highly likely that more methane was produced in the lagoon sediments than is reflected in our results.

5.1.2.3 | CO_2 Dominance Under Increasing Saline Conditions. Our analysis revealed a pronounced dominance in CO_2 production, accounting for 76.0% to 99.9% of the cumulative greenhouse gas production across all samples incubated under brackish and marine conditions (Figure 5e). This suggests that, during and after the transition from terrestrial to marine environments, CO_2 emerged as the primary produced GHG. The highest proportion of CO_2 in cumulative GHG production was observed in LAG2, situated closest to a marine environment and lacking a methanogenic community. Since LAG2 is older than LAG1, it is possible that LAG2 once had a methanogenic community in the past when the lagoon was presumably deeper and did not have the stressful agents it currently possesses, i.e., bottom-fast ice, hyper-salinity, turbidity etc.

In contrast, we measured similar CO_2 and CH_4 production for TPF under freshwater conditions (young lake). This aligns with the findings of Jongejans et al. [31], who reported a similar CH_4:CO_2 production ratio in the surface sediment of an Alas Lake (81.3 µg/gdw CO_2 and 77.1 µg/gdw CH_4). In the surface sediment of the Yedoma Lake, they found a substantial difference, with CH_4 production surpassing CO_2 production (64.1 µg CO_2-C/gdw and 350.2 µg CH_4-C/gdw), which they explained by subsequent gradual population of methanogenic communities due to thaw front migration with talik formation. These

observations emphasize the variability of GHG dynamics in different aquatic habitats and highlight the influence of local conditions on the cumulative CO_2 and CH_4 production.

5.1.2.4 | Short- and Long-Term CO_2 and CH_4 Dynamics.

Our experiment indicates that if TPF or talik sediment is submerged with sea water (scenario F to B in left box of Figure 8), less CO_2 and CH_4 is produced in the short-term due to the lack of microbial communities adapted to the marine environment (see also Figure 6a,b ratios <1). However, in the long-term, after lagoon formation (scenario F in left box to B in right box of Figure 8) and an adaptation period in which SRB (Desulfobacteriota in Figure 3, panel LAG1 and LAG2) and likely marine anaerobic methanotrophic archaea performing AOM are established, CO_2 production increases (Figure 6c ratios >1) and even exceeds CO_2 production in TPF by 8 times (large CO_2 bubble in Figure 8). This suggests that we should expect much higher GHG production in the long-term after lagoon formation. A slightly stronger decrease in CH_4 production from fresh to brackish conditions compared to the decrease from brackish to marine conditions might suggest that the transition from a terrestrial to a saltwater-influenced ecosystem has a greater impact on CH_4 production than the increase in salinity within an established marine ecosystem.

5.1.3 | High Variability in Thermokarst Lake Sediment Production Rates

Surprisingly, our observations revealed no substantial CH_4 and CO_2 production in the sediment of the thermokarst lake regardless of the treatment (with a maximum of $3.13 \pm 0.99\,\mu g$ CO_2-C/gdw measured for TKL-M and a maximum of $1.17 \pm 0.16\,\mu g$ CH_4-C/gdw for TKL-F). This is in contrast with the findings of Jongejans et al. [31], who, under similar incubation conditions (1 year, 4°C, anaerobic), measured considerably higher cumulative greenhouse gas (GHG) production in surface samples from an Alas Lake and a Yedoma Lake in Central Yakutia (ranging from 64.1 to $81.3\,\mu g$ CO_2-C/gdw and 77.1 to $350.3\,\mu g$ CH_4-C/gdw). Furthermore, recent field studies have documented substantial GHG releases from thermokarst lakes in various regions [89, 101, 103–105].

Several potential reasons could account for the observed low productivity in thermokarst Lake Goltsovoye (TKL):

Older age of the talik: The Goltsovoye Lake and its associated talik formed approximately 8000 years BP. Radiocarbon dating of the surface sediment revealed an age of 3600 BP as reported by Jongejans et al. [52], which indicates that the sediment was unfrozen for a long time period. During this time, it is likely that the labile fraction of the OM was decomposed, leading to lower productivity now.

Lack of substrate at the time of coring: A more convincing reason could be the potential lack of substrate at the time of coring at the end of winter. The long winter freezing period likely led to very limited primary production in the lake, resulting in no fresh substrate input from the water column. Microorganisms likely have metabolized easily accessible substrate sources during the winter. Since we did not add nutrients, only electron acceptors for brackish and marine conditions, the experiment started with a very low substrate level.

Low initial microbial colonization: According the qPCR data on gene copy numbers for Goltsovoye Lake (TKL) and Polar Fox Lagoon (LAG1) published by [24] (Figure S4), there are fewer bacteria and sulfate reducers in TKL, but methanogens (mcrA) are similar to those in LAG1. This again might explain the low CO_2 but not the low CH_4 production.

Acidic soil conditions: The low CH_4 production of TKL might be caused by low soil pH, ranging from 4.31 to 5.53 at the start of the incubation (Table S2). Previous studies have shown that
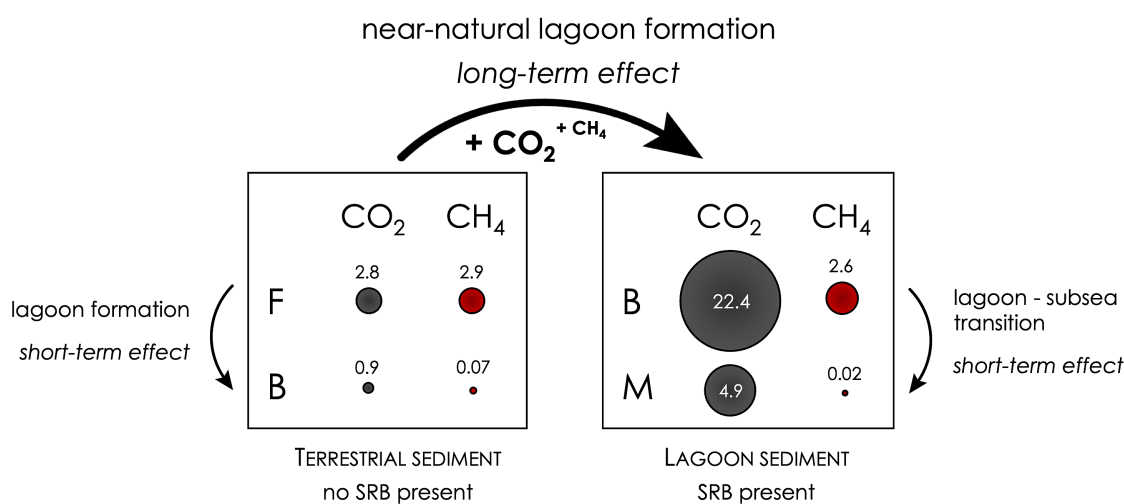

FIGURE 8 | Significant increase in GHG production for lagoon formation under near-natural conditions in the long term by eight-fold from 2.8 to 22.4 mg C gSOC^{-1}. Short-term decrease in GHG production after artificial seawater inundation of terrestrial sediment (left box F → B) or the increase in salinity during the lagoon to subsea transition (right box B → M). The numbers are the mean cumulative CO_2 and CH_4 production (normalized to soil organic carbon content) in mg C gSOC^{-1} under fresh (F) and brackish (B) conditions for terrestrial sites (left box) and brackish and marine (M) conditions for lagoons (right box) after 1-year anaerobic incubation. The bubble size is proportional to the cumulative production. [Colour figure can be viewed at wileyonlinelibrary.com]

extreme pH values negatively affect microbial biomass and activity [106] and can suppress methanogenesis by 71.7% for a pH of 5.5 or even up to 100% for a pH of 4 [107]. However, by the end of the incubation, pH values for TKL and TPF were similar, suggesting the low pH alone does not explain the difference in CH_4 production.

5.1.4 | Limitations of Incubation Experiments

Laboratory incubations have several limitations. Microcosm incubations under lab conditions often fail to replicate complex environmental conditions, spatial heterogeneity, and microbial communities. Controlled settings are needed to examine the separate influences of specific parameters, such as salinity in our case, but they overlook dynamic natural changes, and microbial communities may shift during incubation. Abiotic interactions and the absence of plant–soil interactions are inadequately represented in microcosms. These factors lead to potential inaccuracies in predicting long-term, large-scale GHG emissions. However, laboratory incubations still provide valuable insights into the mechanisms of GHG production in permafrost.

5.2 | Proposed Microbial Responses and GHG Dynamics in Changing Coastal Permafrost Landscapes

Coastal permafrost landscapes are dynamic environments that undergo significant changes over time [14, 20, 108–111]. Understanding the stages from thawing TPF over lake and lagoon formation towards the full submergence in the subsea stage is crucial for understanding the associated GHG production (Figure 9). In open systems, the input of nutrients and dissolved and particulate OC promotes microbial growth. Further, the input of marine microorganisms through inundating seawater and transported sediment would promote initial colonization by, for example, SRB and potentially anaerobic methane oxidizers, which will likely accelerate the shift from CH_4 to CO_2 production in land-sea transitioning systems. On the other hand, the

export of OC in the form of DOC and particulate OC through leaching and erosion could result in a decrease in the availability of easily degradable OM especially in lagoons. Input of pollutants such as mercury, which tend to enrich in thermokarst features [112–114] could inhibit microbial growth and thus lead to decreased CO_2 and CH_4 production. These are just a few examples of processes impacting GHG production in nature; however, it is not possible to integrate all of them in incubation experiments. While acknowledging the inherent limitations of small-scale laboratory experiments in replicating the complexity of the real world, these experiments can provide valuable insights into potential responses. Moreover, the comparison of II, IIIa, and IIIb (TKL, LAG1 and LAG2 respectively) is made possible by their close proximity and the similar genesis of the sites [19, 24, 53]. Although more distant, Site I (TPF) serves as a valuable endmember.

Thawing of ice-rich permafrost for the first time and the formation of a thaw pond or a young thermokarst lake triggers substantial GHG production (Figure 9 panel I). Our data suggest that both CO_2 and CH_4 are likely produced in equal amounts during this phase. After the long existence of thermokarst lakes, such as Goltsovoye TKL (panel II), a significant reduction in GHG production was observed in the surface sediment.

Following drainage, as the lake established a connection to the sea, nearly enclosed lagoons like Polar Fox LAG1 (panel IIIa) show very high CO_2 production along with substantial CH_4 production. Due to the limited connectivity, OC-rich materials eroded from the Yedoma uplands and the shoreline are captured. Rich substrate availability and moderate salinity facilitate high microbial diversity and the coexistence of methanogens and sulfate-reducing organisms.

With time and landward migration of the sea, the lagoon becomes more strongly connected (panel IIIb: semi-open lagoon Uomullyakh [LAG2]). Increased marine sediment influx may lead to shallowing of the lagoon, resulting in seasonally frozen and increasingly saline ground. This environmental stressor triggers a decline in microbial abundance. Increased sulfate
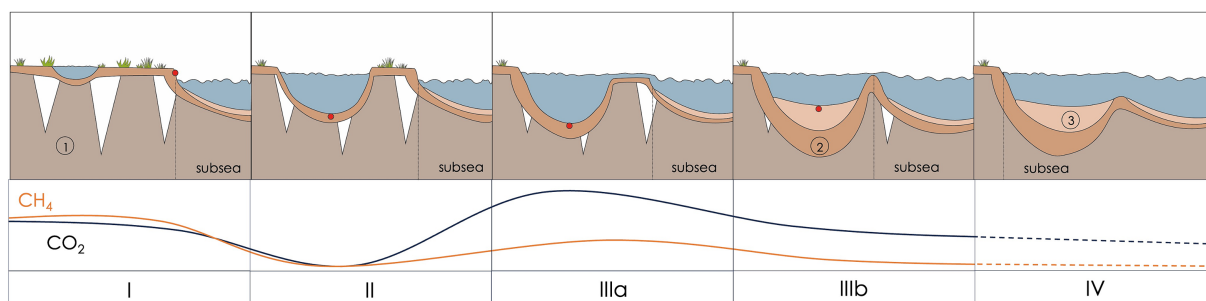

FIGURE 9 | Generalized illustration of coastal landscape development in the study area and possible greenhouse gas production at each stage of development. I: Thaw pond forming on terrestrial, ice-rich permafrost (outcrop TPF), II: advanced lake formation due to ongoing local permafrost thaw (old thermokarst lake Goltsovoye TKL), IIIa: first stage of lagoon formation—lake is connected to the sea via a channel with limited exchange (nearly closed lagoon Polar Fox LAG1), IIIb: older lagoon, more strongly connected to the sea (semi-open lagoon Uomullyakh LAG2), and IV: subsea after erosion of the land barrier. Red dots show sampling locations. ① frozen ground with ice wedges; ② active layer and talik; ③ marine sediment. CO_2 and CH_4 lines illustrate the production potential during that phase of landscape development based on cumulative production measured during the incubation experiment for the near natural conditions of the corresponding phase (freshwater for I and II, brackish for IIIa and IIIb, GHG production in subsea sediment IV is unknown, but the trend is based on cumulative GHG production of LAG2 (IIIb) under marine conditions). [Colour figure can be viewed at wileyonlinelibrary.com]

input induces a shift in microbial communities, favoring the growth of SRB and a significant increase in CO_2 production compared to CH_4. A recent study by Jones et al. [115] suggests that the frequency of lake drainage events is rising due to changing hydrological patterns. This shift may result in a higher occurrence of nearly closed lagoon formation along Arctic coasts, intensifying both CO_2 and CH_4 production. Rising sea level leading to complete submersion of the lagoon into subsea marks the final stage. Although CO_2 and CH_4 production was not measured directly in subsea sediments, trends can be derived from the cumulative greenhouse gas production in semi-open lagoon sediments (LAG2) under marine conditions showing a further decrease in GHG production.

Summing up, our data suggest that the dynamics of lagoon formation and its implications for CO_2 and CH_4 production unveil a nuanced relationship between microbial adaptation and greenhouse gas production. During the initial stages of permafrost sediment transitioning into a more marine environment through lagoon formation, new microbial communities have to evolve, leading to an initial reduction of CO_2 and CH_4 production. However, with an adaptation period marked by the establishment of SRB, CO_2 production undergoes a significant increase, surpassing levels observed in thawed TPF by about 8 times. Once SRB are established, methane production plays a secondary role.

Our marine lab experiments resulted in lower CO_2 production than other scenarios, indicating an incomplete adaptation of lagoon systems to marine conditions. This underscores the existence of a transition period during ecosystem shifts. Moreover, under near-natural conditions, where microbial organisms are likely optimally adapted, GHG production peaks at all sites.

Our results highlight that nearly closed thermokarst lagoons, partially connected to the sea and largely undisturbed by wave action, currents, and marine sediment influx, exhibit particularly high CO_2 production per gram of dry weight. Conversely, more open lagoons characterized by marine sediment influx demonstrate lower OC contents but appear to produce similar amounts of CO_2 if normalized to the OM content. These types of lagoons represent the first stages of the transition from lake to subsea. With an increase in lake drainage events and rising sea level, the distribution of thermokarst lagoons on Arctic coasts will escalate, resulting in further rising carbon mineralization and GHG release at the coast. This emphasizes the crucial role of microbial adaptation in shaping the carbon cycle and GHG emissions in permafrost-affected coastal environments.

6 | Conclusion

Our incubation study of sediment samples from a depositional gradient—from TPF to freshwater thermokarst lakes to thermokarst lagoons—revealed that permafrost sediments inundated and thawed by seawater initially produce less CO_2 in the short term due to the delayed establishment of marine/salt-adapted microbial communities. Once SRB adapt, CO_2 production increases, exceeding TPF levels by eightfold. Despite this, the marine scenario produces less CO_2 and CH_4 than the other scenarios, indicating that coastal systems are not fully adapted to marine conditions. This transition requires time for microbial adaptation, impacting

biogeochemical cycling. We found GHG production to be highest in near-natural conditions, freshwater for terrestrial sites and brackish for lagoons, where microorganisms are best adapted. Our findings highlight the complex interplay of microbial processes and environmental transitions at the land-sea boundary in permafrost regions. While acknowledging the limitations of lab-scale experiments in fully capturing landscape and microbial processes, our approach enhances the understanding of climate change and carbon dynamics in permafrost coastal ecosystems.

Conflicts of Interest

The authors declare no conflicts of interest.

Data Availability Statement

The dataset on the cumulative GHG production and the productions rates can be found in the online repository PANGAEA (10.1594/PANGAEA.967267). The DNA data for this study have been deposited in the European Nucleotide Archive (ENA) at EMBL-EBI under project accession number PRJEB49195 with sample accession numbers ERS18087194-ERS18087223.

References

1. J. Obu, "How Much of the Earth's Surface Is Underlain by Permafrost?," *Journal of Geophysical Research - Earth Surface* 126 (2021): e2021JF006123, https://doi.org/10.1029/2021JF006123.

2. P. P. Overduin, T. Schneider von Deimling, F. Miesner, et al., "Submarine Permafrost Map in the Arctic Modeled Using 1-D Transient Heat Flux (SuPerMAP)," *Journal of Geophysical Research, Oceans* 124 (2019): 3490–3507, https://doi.org/10.1029/2018JC014675.

3. A. Lindgren, G. Hugelius, and P. Kuhry, "Extensive Loss of Past Permafrost Carbon But a Net Accumulation Into Present-Day Soils," *Nature* 560 (2018): 219–222, https://doi.org/10.1038/s41586-018-0371-0.

4. K. R. Miner, M. R. Turetsky, E. Malina, et al., "Permafrost Carbon Emissions in a Changing Arctic," *Nature Reviews Earth and Environment* 3 (2022): 55–67, https://doi.org/10.1038/s43017-021-00230-3.

5. E. A. G. Schuur, B. W. Abbott, R. Commane, et al., "Permafrost and Climate Change: Carbon Cycle Feedbacks From the Warming Arctic [WWW Document]," (2022), https://doi.org/10.1146/annurev-environ-012220-011847.

6. K. M. W. Anthony, S. A. Zimov, G. Grosse, et al., "A Shift of Thermokarst Lakes From Carbon Sources to Sinks During the Holocene Epoch," *Nature* 511 (2014): 452–456, https://doi.org/10.1038/nature13560.

7. J. Strauss, S. Laboor, L. Schirrmeister, et al., "Circum-Arctic Map of the Yedoma Permafrost Domain," *Frontiers in Earth Science* 9 (2021): 758360, https://doi.org/10.3389/feart.2021.758360.

8. F. Miesner, P. P. Overduin, G. Grosse, et al., "Subsea Permafrost Organic Carbon Stocks Are Large and of Dominantly Low Reactivity," *Scientific Reports* 13 (2023): 9425, https://doi.org/10.1038/s41598-023-36471-z.

9. M. Rantanen, A. Y. Karpechko, A. Lipponen, et al., "The Arctic Has Warmed Nearly Four Times Faster Than the Globe Since 1979," *Communications Earth & Environment* 3 (2022): 168, https://doi.org/10.1038/s43247-022-00498-3.

10. S. Wilkenskjeld, F. Miesner, P. P. Overduin, M. Puglini, and V. Brovkin, "Strong Increase in Thawing of Subsea Permafrost in the 22nd Century Caused by Anthropogenic Climate Change," *The Cryosphere* 16 (2022): 1057–1069, https://doi.org/10.5194/tc-16-1057-2022.

11. S. M. Natali, J. D. Watts, B. M. Rogers, et al., "Large Loss of CO_2 in Winter Observed Across the Northern Permafrost Region," *Nature Climate Change* 9 (2019): 852–857, https://doi.org/10.1038/s41558-019-0592-8.

12. F. Günther, P. P. Overduin, A. V. Sandakov, G. Grosse, and M. N. Grigoriev, "Short- and Long-Term Thermo-Erosion of ice-Rich Permafrost Coasts in the Laptev Sea Region," *Biogeosciences* 10 (2013): 4297–4318, https://doi.org/10.5194/bg-10-4297-2013.

13. B. M. Jones, L. M. Farquharson, C. A. Baughman, et al., "A Decade of Remotely Sensed Observations Highlight Complex Processes Linked to Coastal Permafrost Bluff Erosion in the Arctic," *Environmental Research Letters* 13 (2018): 115001, https://doi.org/10.1088/1748-9326/aae471.

14. D. M. Nielsen, P. Pieper, A. Barkhordarian, et al., "Increase in Arctic Coastal Erosion and Its Sensitivity to Warming in the Twenty-First Century," *Nature Climate Change* 12 (2022): 263–270, https://doi.org/10.1038/s41558-022-01281-0.

15. J. A. Guimond, A. A. Mohammed, M. A. Walvoord, V. F. Bense, and B. L. Kurylyk, "Saltwater Intrusion Intensifies Coastal Permafrost Thaw," *Geophysical Research Letters* 48 (2021): e2021GL094776, https://doi.org/10.1029/2021GL094776.

16. R. S. Nerem, B. D. Beckley, J. T. Fasullo, B. D. Hamlington, D. Masters, and G. T. Mitchum, "Climate-Change-Driven Accelerated Sea-Level Rise Detected in the Altimeter Era," *Proceedings of the National Academy of Sciences of the United States of America* 115 (2018): 2022–2025, https://doi.org/10.1073/pnas.1717312115.

17. A. Proshutinsky, V. Pavlov, and R. H. Bourke, "Sea Level Rise in the Arctic Ocean," *Geophysical Research Letters* 28 (2001): 2237–2240, https://doi.org/10.1029/2000GL012760.

18. C. S. Watson, N. J. White, J. A. Church, M. A. King, R. J. Burgette, and B. Legresy, "Unabated Global Mean Sea-Level Rise Over the Satellite Altimeter Era," *Nature Climate Change* 5 (2015): 565–568, https://doi.org/10.1038/nclimate2635.

19. M. Jenrich, M. Angelopoulos, G. Grosse, et al., "Thermokarst Lagoons: A Core-Based Assessment of Depositional Characteristics and an Estimate of Carbon Pools on the Bykovsky Peninsula," *Frontiers in Earth Science* 9 (2021): 637899, https://doi.org/10.3389/feart.2021.637899.

20. A. M. Irrgang, M. Bendixen, L. M. Farquharson, et al., "Drivers, Dynamics and Impacts of Changing Arctic Coasts," *Nature Reviews Earth and Environment* 3 (2022): 39–54, https://doi.org/10.1038/s43017-021-00232-1.

21. C. M. Harris, J. W. McClelland, T. L. Connelly, B. C. Crump, and K. H. Dunton, "Salinity and Temperature Regimes in Eastern Alaskan Beaufort Sea Lagoons in Relation to Source Water Contributions," *Estuaries and Coasts* 40 (2017): 50–62, https://doi.org/10.1007/s12237-016-0123-z.

22. B. Kjerfve, "Chapter 1 Coastal Lagoons," in *Elsevier Oceanography Series, Coastal Lagoon Processes*, ed. B. Kjerfve (Elsevier Science Publisher B.V., 1994): 1–8, https://doi.org/10.1016/S0422-9894(08)70006-0.

23. D. Tagliapietra, M. Sigovini, and A. Volpi Ghirardini, "A Review of Terms and Definitions to Categorise Estuaries, Lagoons and Associated Environments," *Marine and Freshwater Research* 60 (2009): 497–509, https://doi.org/10.1071/MF08088.

24. S. Yang, S. E. Anthony, M. Jenrich, et al., "Microbial Methane Cycling in Sediments of Arctic Thermokarst Lagoons," *Global Change Biology* 29 (2023): 2714–2731, https://doi.org/10.1111/gcb.16649.

25. I. Spangenberg, P. P. Overduin, E. Damm, et al., "Methane Pathways in Winter Ice of a Thermokarst Lake–Lagoon–Coastal Water Transect in North Siberia," *The Cryosphere* 15 (2021): 1607–1625, https://doi.org/10.5194/tc-15-1607-2021.

26. M. Angelopoulos, P. P. Overduin, F. Miesner, M. N. Grigoriev, and A. A. Vasiliev, "Recent Advances in the Study of Arctic Submarine Permafrost," *Permafrost and Periglacial Processes* 31 (2020a): 442–453, https://doi.org/10.1002/ppp.2061.

27. M. Laurent, M. Fuchs, T. Herbst, A. Runge, S. Liebner, and C. C. Treat, "Relationships Between Greenhouse Gas Production and Landscape Position During Short-Term Permafrost Thaw Under Anaerobic Conditions in the Lena Delta," *Biogeosciences* 20 (2023): 2049–2064, https://doi.org/10.5194/bg-20-2049-2023.

28. G. Tanski, D. Wagner, C. Knoblauch, M. Fritz, T. Sachs, and H. Lantuit, "Rapid CO_2 Release From Eroding Permafrost in Seawater," *Geophysical Research Letters* 46 (2019): 11244–11252, https://doi.org/10.1029/2019GL084303.

29. C. Knoblauch, C. Beer, A. Sosnin, D. Wagner, and E.-M. Pfeiffer, "Predicting Long-Term Carbon Mineralization and Trace Gas Production From Thawing Permafrost of Northeast Siberia," *Global Change Biology* 19 (2013): 1160–1172, https://doi.org/10.1111/gcb.12116.

30. C. C. Treat, S. M. Natali, J. Ernakovich, et al., "A Pan-Arctic Synthesis of CH_4 and CO_2 Production From Anoxic Soil Incubations," *Global Change Biology* 21 (2015): 2787–2803, https://doi.org/10.1111/gcb.12875.

31. L. L. Jongejans, S. Liebner, C. Knoblauch, et al., "Greenhouse Gas Production and Lipid Biomarker Distribution in Yedoma and Alas Thermokarst Lake Sediments in Eastern Siberia," *Global Change Biology* 27 (2021): 2822–2839, https://doi.org/10.1111/gcb.15566.

32. C. Schädel, M. K.-F. Bader, E. A. G. Schuur, et al., "Potential Carbon Emissions Dominated by Carbon Dioxide From Thawed Permafrost Soils," *Nature Climate Change* 6 (2016): 950–953, https://doi.org/10.1038/nclimate3054.

33. L. de Galera, T. Eckhardt, C. Beer, E.-M. Pfeiffer, and C. Knoblauch, "Ratio of in Situ CO_2 to CH_4 Production and Its Environmental Controls in Polygonal Tundra Soils of Samoylov Island, Northeastern Siberia," *Journal of Geophysical Research: Biogeosciences* 128 (2023): e2022JG006956, https://doi.org/10.1029/2022JG006956.

34. J.k. Heslop, M. Winkel, K.m. Walter Anthony, et al., "Increasing Organic Carbon Biolability With Depth in Yedoma Permafrost: Ramifications for Future Climate Change," *Journal of Geophysical Research: Biogeosciences* 124 (2019): 2021–2038, https://doi.org/10.1029/2018JG004712.

35. J. K. Heslop, K. M. Walter Anthony, A. Sepulveda-Jauregui, et al., "Thermokarst Lake Methanogenesis Along a Complete Talik Profile," *Biogeosciences* 12 (2015): 4317–4331, https://doi.org/10.5194/bg-12-4317-2015.

36. J. K. Heslop, K. M. Walter Anthony, M. Winkel, et al., "A Synthesis of Methane Dynamics in Thermokarst Lake Environments," *Earth Science Reviews* 210 (2020): 103365, https://doi.org/10.1016/j.earscirev.2020.103365.

37. C. Knoblauch, C. Beer, S. Liebner, M. N. Grigoriev, and E.-M. Pfeiffer, "Methane Production as Key to the Greenhouse Gas Budget of Thawing Permafrost," *Nature Climate Change* 8 (2018): 309–312, https://doi.org/10.1038/s41558-018-0095-z.

38. P. Kuhry, J. Bárta, D. Blok, et al., "Lability Classification of Soil Organic Matter in the Northern Permafrost Region," *Biogeosciences* 17 (2020): 361–379, https://doi.org/10.5194/bg-17-361-2020.

39. H. Lee, E. A. G. Schuur, K. S. Inglett, M. Lavoie, and J. P. Chanton, "The Rate of Permafrost Carbon Release Under Aerobic and Anaerobic Conditions and Its Potential Effects on Climate," *Global Change Biology* 18 (2012): 515–527, https://doi.org/10.1111/j.1365-2486.2011.02519.x.

40. D. E. Holmes, P. M. Shrestha, D. J. F. Walker, et al., "Metatranscriptomic Evidence for Direct Interspecies Electron Transfer Between Geobacter and Methanothrix Species in Methanogenic Rice Paddy Soils," *Applied and Environmental Microbiology* 83 (2017): e00223, https://doi.org/10.1128/AEM.00223-17.

41. J. K. Kristjansson and P. Schönheit, "Why Do Sulfate-Reducing Bacteria Outcompete Methanogenic Bacteria for Substrates?," *Oecologia* 60 (1983): 264–266.

42. D. R. Lovley, D. F. Dwyer, and M. J. Klug, "Kinetic Analysis of Competition Between Sulfate Reducers and Methanogens for Hydrogen in Sediments," *Applied and Environmental Microbiology* 43 (1982): 1373–1379, https://doi.org/10.1128/aem.43.6.1373-1379.1982.

43. D. Olefeldt, M. R. Turetsky, P. M. Crill, and A. D. McGuire, "Environmental and Physical Controls on Northern Terrestrial Methane Emissions Across Permafrost Zones," *Global Change Biology* 19 (2013): 589–603, https://doi.org/10.1111/gcb.12071.

44. P. Schönheit, J. K. Kristjansson, and R. K. Thauer, "Kinetic Mechanism for the Ability of Sulfate Reducers to Out-Compete Methanogens for Acetate," *Archives of Microbiology* 132 (1982): 285–288, https://doi.org/10.1007/BF00407967.

45. C. N. Gutekunst, S. Liebner, A.-K. Jenner, et al., "Effects of Brackish Water Inflow on Methane-Cycling Microbial Communities in a Freshwater Rewetted Coastal Fen," *Biogeosciences* 19 (2022): 3625–3648, https://doi.org/10.5194/bg-19-3625-2022.

46. J. K. Jansson and K. S. Hofmockel, "The Soil Microbiome—From Metagenomics to Metaphenomics," *Current Opinion in Microbiology* 43 (2018): 162–168, https://doi.org/10.1016/j.mib.2018.01.013.

47. L. Schirrmeister, G. Grosse, S. Wetterich, et al., "Fossil Organic Matter Characteristics in Permafrost Deposits of the Northeast Siberian Arctic," *Journal of Geophysical Research: Biogeosciences* 116 (2011), https://doi.org/10.1029/2011JG001647.

48. L. Schirrmeister, C. Siegert, T. Kuznetsova, et al., "Paleoenvironmental and Paleoclimatic Records From Permafrost Deposits in the Arctic Region of Northern Siberia," *Quaternary International* 89 (2002): 97–118, https://doi.org/10.1016/S1040-6182(01)00083-0.

49. A. V. Sher, S. A. Kuzmina, T. V. Kuznetsova, and L. D. Sulerzhitsky, "New Insights Into the Weichselian Environment and Climate of the East Siberian Arctic, Derived From Fossil Insects, Plants, and Mammals," *Quaternary Science Reviews* 24 (2005): 533–569, https://doi.org/10.1016/j.quascirev.2004.09.007.

50. G. Grosse, A. Morgenstern, and H. Lantuit, "Distribution of Thermokarst Lakes and Ponds at Three Yedoma Sites in Siberia," Presented at the NINTH INTERNATIONAL CONFERENCE ON PERMAFROST (2008).

51. G. Grosse, L. Schirrmeister, V. V. Kunitsky, and H.-W. Hubberten, "The Use of CORONA Images in Remote Sensing of Periglacial Geomorphology: An Illustration From the NE Siberian Coast," *Permafrost and Periglacial Processes* 16 (2005): 163–172, https://doi.org/10.1002/ppp.509.

52. L. L. Jongejans, K. Mangelsdorf, L. Schirrmeister, et al., "N-Alkane Characteristics of Thawed Permafrost Deposits Below a Thermokarst Lake on Bykovsky Peninsula, Northeastern Siberia," *Frontiers in Environmental Science* 8 (2020): 118, https://doi.org/10.3389/fenvs.2020.00118.

53. M. Angelopoulos, P. P. Overduin, S. Westermann, et al., "Thermokarst Lake to Lagoon Transitions in Eastern Siberia: Do Submerged Taliks Refreeze?," *Journal of Geophysical Research - Earth Surface* 125 (2020b): e2019JF005424, https://doi.org/10.1029/2019JF005424.

54. M. Fuchs, G. Grosse, J. Strauss, et al., "Carbon and Nitrogen Pools in Thermokarst-Affected Permafrost Landscapes in Arctic Siberia," *Biogeosciences* 15 (2018): 953–971, https://doi.org/10.5194/bg-15-953-2018.

55. U. Mishra, G. Hugelius, E. Shelef, et al., "Spatial Heterogeneity and Environmental Predictors of Permafrost Region Soil Organic Carbon Stocks," *Science Advances* 7 (2021): eaaz5236, https://doi.org/10.1126/sciadv.aaz5236.

56. M. Angelopoulos, "Mapping Subsea Permafrost With Electrical Resistivity Surveys," *Nature Reviews Earth and Environment* 3 (2022): 6, https://doi.org/10.1038/s43017-021-00258-5.

57. M. Angelopoulos, P. P. Overduin, M. Jenrich, et al., "Onshore Thermokarst Primes Subsea Permafrost Degradation," *Geophysical Research Letters* 48 (2021): e2021GL093881, https://doi.org/10.1029/2021GL093881.

58. M. Angelopoulos, S. Westermann, P. Overduin, et al., "Heat and Salt Flow in Subsea Permafrost Modeled With CryoGRID2," *Journal of Geophysical Research - Earth Surface* 124 (2019): 920–937, https://doi.org/10.1029/2018JF004823.

59. M. Arboleda-Zapata, M. Angelopoulos, P. P. Overduin, G. Grosse, B. M. Jones, and J. Tronicke, "Exploring the Capabilities of Electrical Resistivity Tomography to Study Subsea Permafrost," *The Cryosphere* 16 (2022): 4423–4445, https://doi.org/10.5194/tc-16-4423-2022.

60. V. V lenchenko, A. N. Faguet, P. P. Overduin, and M. Angelopoulos, "Geoelectric Structure of the Subaquatic Cryolithozone in Uumullakh-Kyuel Lagoon (Laptev Sea)," *Earth's Cryosphere* (2023): 5 (in Russian), https://doi.org/10.15372/KZ20230504.

61. J. Strauss, J. Boike, D. Y. Bolshiyanov, et al., "Russian-German Cooperation: Expeditions to Siberia in 2017, Berichte zur Polar- Und Meeresforschung = Reports on Polar and Marine Research," *Alfred-Wegener-Institut, Helmholtz-Zentrum für Polar- Und Meeresforschung* (2018): 122–138, https://doi.org/10.2312/BZPM_0725_2018.

62. T. J. McDougall and P. M. Barker, Getting Started With TEOS-10 and the Gibbs Seawater (GSW) Oceanographic Toolbox (2011), 28 pp., SCOR/IAPSO WG127, ISBN 978-0-646-55621-5.

63. F. J. Millero, R. Feistel, D. G. Wright, and T. J. McDougall, "The Composition of Standard Seawater and the Definition of the Reference-Composition Salinity Scale," *Deep Sea Research Part I: Oceanographic Research Papers* 55 (2008): 50–72, https://doi.org/10.1016/j.dsr.2007.10.001.

64. M. Fritz, T. Opel, G. Tanski, et al., "Dissolved Organic Carbon (DOC) in Arctic Ground ice," *The Cryosphere* 9 (2015): 737–752, https://doi.org/10.5194/tc-9-737-2015.

65. S. J. Blott and K. Pye, "GRADISTAT: A Grain Size Distribution and Statistics Package for the Analysis of Unconsolidated Sediments," *Earth Surface Processes and Landforms* 26 (2001): 1237–1248, https://doi.org/10.1002/esp.261.

66. P. P. Overduin, S. Wetterich, F. Günther, et al., "Coastal Dynamics and Submarine Permafrost in Shallow Water of the Central Laptev Sea, East Siberia," *The Cryosphere* 10 (2016): 1449–1462, https://doi.org/10.5194/tc-10-1449-2016.

67. J. A. Crawshaw, M. Schallenberg, and C. Savage, "Physical and Biological Drivers of Sediment Oxygenation and Denitrification in a New Zealand Intermittently Closed and Open Lake Lagoon," *New Zealand Journal of Marine and Freshwater Research* 53 (2019): 33–59, https://doi.org/10.1080/00288330.2018.1476388.

68. F. Millero, F. Huang, T. Graham, and D. Pierrot, "The Dissociation of Carbonic Acid in NaCl Solutions as a Function of Concentration and Temperature," *Geochimica et Cosmochimica Acta* 71 (2007): 46–55, https://doi.org/10.1016/j.gca.2006.08.041.

69. M. Martin, "Cutadapt Removes Adapter Sequences From High-Throughput Sequencing Reads," *EMBnet.Journal* 17 (2011): 10–12, https://doi.org/10.14806/ej.17.1.200.

70. B. J. Callahan, P. J. McMurdie, M. J. Rosen, A. W. Han, A. J. A. Johnson, and S. P. Holmes, "DADA2: High-Resolution Sample Inference From Illumina Amplicon Data," *Nature Methods* 13 (2016): 581–583, https://doi.org/10.1038/nmeth.3869.

71. C. Quast, E. Pruesse, P. Yilmaz, et al., "The SILVA Ribosomal RNA Gene Database Project: Improved Data Processing and Web-Based Tools," *Nucleic Acids Research* 41 (2013): D590–D596, https://doi.org/10.1093/nar/gks1219.

72. J. Oksanen, G. Simpson, F. G. Blanchet, et al., vegan Community Ecology Package Version 2.6-2 April 2022.

73. H. Wickham, ggplot2, Use R! (Cham: Springer International Publishing, 2016), https://doi.org/10.1007/978-3-319-24277-4.

74. S. Yang, S. Liebner, J. Walz, et al., "Effects of a Long-Term Anoxic Warming Scenario on Microbial Community Structure and Functional Potential of Permafrost-Affected Soil," *Permafrost and Periglacial Processes* 32 (2021): 641–656, https://doi.org/10.1002/ppp.2131.

75. J. G. Ernakovich, R. A. Barbato, V. I. Rich, et al., "Microbiome Assembly in Thawing Permafrost and Its Feedbacks to Climate," *Global Change Biology* 28 (2022): 5007–5026, https://doi.org/10.1111/gcb.16231.

76. R. A. Barbato, R. M. Jones, T. A. Douglas, et al., "Not All Permafrost Microbiomes Are Created Equal: Influence of Permafrost Thaw on the Soil Microbiome in a Laboratory Incubation Study," *Soil Biology and Biochemistry* 167 (2022): 108605, https://doi.org/10.1016/j.soilbio.2022.108605.

77. M. J. L. Coolen and W. D. Orsi, "The Transcriptional Response of Microbial Communities in Thawing Alaskan Permafrost Soils," *Frontiers in Microbiology* 6 (2015): 6.

78. M. J. L. Coolen, J. van de Giessen, E. Y. Zhu, and C. Wuchter, "Bioavailability of Soil Organic Matter and Microbial Community Dynamics Upon Permafrost Thaw," *Environmental Microbiology* 13 (2011): 2299–2314, https://doi.org/10.1111/j.1462-2920.2011.02489.x.

79. R. Mackelprang, M. P. Waldrop, K. M. DeAngelis, et al., "Metagenomic Analysis of a Permafrost Microbial Community Reveals a Rapid Response to Thaw," *Nature* 480 (2011): 368–371, https://doi.org/10.1038/nature10576.

80. V. A. Lyubetsky, O. A. Zverkov, L. I. Rubanov, and A. V. Seliverstov, "Optimal Growth Temperature and Intergenic Distances in Bacteria, Archaea, and Plastids of Rhodophytic Branch," *BioMed Research International* 2020 (2020): 3465380, https://doi.org/10.1155/2020/3465380.

81. J. Mitzscherling, F. Horn, M. Winterfeld, et al., "Microbial Community Composition and Abundance After Millennia of Submarine Permafrost Warming," *Biogeosciences* 16 (2019): 3941–3958, https://doi.org/10.5194/bg-16-3941-2019.

82. M. A. Khomyakova, D. G. Zavarzina, A. Y. Merkel, et al., "The First Cultivated Representatives of the Actinobacterial Lineage OPB41 Isolated From Subsurface Environments Constitute a Novel Order Anaerosomatales," *Frontiers in Microbiology* 13 (2022): 1047580, https://doi.org/10.3389/fmicb.2022.1047580.

83. S. Dyksma and M. Pester, "Oxygen Respiration and Polysaccharide Degradation by a Sulfate-Reducing Acidobacterium," *Nature Communications* 14 (2023): 6337, https://doi.org/10.1038/s41467-023-42074-z.

84. D. Ozuolmez, E. K. Moore, E. C. Hopmans, J. S. Sinninghe Damsté, A. J. M. Stams, and C. M. Plugge, "Butyrate Conversion by Sulfate-Reducing and Methanogenic Communities From Anoxic Sediments of Aarhus Bay, Denmark," *Microorganisms* 8 (2020): 606, https://doi.org/10.3390/microorganisms8040606.

85. D. Ozuolmez, H. Na, M. Lever, K. Kjeldsen, B. Jørgensen, and C. Plugge, "Methanogenic Archaea and Sulfate Reducing Bacteria Co-Cultured on Acetate: Teamwork or Coexistence?," *Frontiers in Microbiology* 6 (2015): 6.

86. M. Sela-Adler, Z. Ronen, B. Herut, et al., "Co-Existence of Methanogenesis and Sulfate Reduction With Common Substrates in Sulfate-Rich Estuarine Sediments," *Frontiers in Microbiology* 8 (2017): 8.

87. D. Zona, D. A. Lipson, U. K. T. Paw, et al., "Increased CO_2 Loss From Vegetated Drained Lake Tundra Ecosystems due to Flooding," *Global Biogeochemical Cycles* 26, no. 2 (2012), https://doi.org/10.1029/2011GB004037.

88. T. R. Moore and M. Dalva, "Methane and Carbon Dioxide Exchange Potentials of Peat Soils in Aerobic and Anaerobic Laboratory Incubations," *Soil Biology and Biochemistry* 29 (1997): 1157–1164, https://doi.org/10.1016/S0038-0717(97)00037-0.

89. E. A. G. Schuur, J. Bockheim, J. G. Canadell, et al., "Vulnerability of Permafrost Carbon to Climate Change: Implications for the Global Carbon Cycle," *BioScience* 58 (2008): 701–714, https://doi.org/10.1641/B580807.

90. V. Bischoff, "Carbon Degradation and Potential Greenhouse Gas Production in a Changing Arctic Thermokarst Landscape—A Case Study From Drained Lake Basins on the Yukon Coastal Plain, Canada" (master's thesis, RWTH Aachen University, Germany, 2024).

91. M. Jenrich, J. Wolter, S. Liebner, et al., "Rising Arctic Seas and Thawing Permafrost: Uncovering the Carbon Cycle Impact in a Thermokarst Lagoon System in the Outer Mackenzie Delta, Canada," (in submission).

92. R. Akinyede, M. Taubert, M. Schrumpf, S. Trumbore, and K. Küsel, "Rates of Dark CO_2 Fixation Are Driven by Microbial Biomass in a Temperate Forest Soil," *Soil Biology and Biochemistry* 150 (2020): 107950, https://doi.org/10.1016/j.soilbio.2020.107950.

93. H. Šantrůčková, P. Kotas, J. Bárta, et al., "Significance of Dark CO_2 Fixation in Arctic Soils," *Soil Biology and Biochemistry* 119 (2018): 11–21, https://doi.org/10.1016/j.soilbio.2017.12.021.

94. F. Beulig, T. Urich, M. Nowak, et al., "Altered Carbon Turnover Processes and Microbiomes in Soils Under Long-Term Extremely High CO_2 Exposure," *Nature Microbiology* 1 (2016): 1–10, https://doi.org/10.1038/nmicrobiol.2015.25.

95. M. Spohn, K. Müller, C. Höschen, C. W. Mueller, and S. Marhan, "Dark Microbial CO_2 Fixation in Temperate Forest Soils Increases With CO_2 Concentration," *Global Change Biology* 26 (2020): 1926–1935, https://doi.org/10.1111/gcb.14937.

96. C. C. Treat, W. M. Wollheim, R. K. Varner, A. S. Grandy, J. Talbot, and S. Frolking, "Temperature and Peat Type Control CO_2 and CH_4 Production in Alaskan Permafrost Peats," *Global Change Biology* 20 (2014): 2674–2686, https://doi.org/10.1111/gcb.12572.

97. M. P. Waldrop, K. P. Wickland, R. White Iii, A. A. Berhe, J. W. Harden, and V. E. Romanovsky, "Molecular Investigations Into a Globally Important Carbon Pool: Permafrost-Protected Carbon in Alaskan Soils," *Global Change Biology* 16 (2010): 2543–2554, https://doi.org/10.1111/j.1365-2486.2009.02141.x.

98. M. Lupascu, J. L. Wadham, E. R. C. Hornibrook, and R. D. Pancost, "Temperature Sensitivity of Methane Production in the Permafrost Active Layer at Stordalen, Sweden: A Comparison With Non-Permafrost Northern Wetlands," *Arctic, Antarctic, and Alpine Research* 44 (2012): 469–482, https://doi.org/10.1657/1938-4246-44.4.469.

99. P. M. J. Douglas, R. Gonzalez Moguel, K. M. Walter Anthony, et al., "Clumped Isotopes Link Older Carbon Substrates With Slower Rates of

Methanogenesis in Northern Lakes," *Geophysical Research Letters* 47 (2020): e2019GL086756, https://doi.org/10.1029/2019GL086756.

100. C. D. Elder, X. Xu, J. Walker, et al., "Greenhouse Gas Emissions From Diverse Arctic Alaskan Lakes Are Dominated by Young Carbon," *Nature Climate Change* 8 (2018): 166–171, https://doi.org/10.1038/s41558-017-0066-9.

101. K. Walter Anthony, T. Schneider von Deimling, I. Nitze, et al., "21st-Century Modeled Permafrost Carbon Emissions Accelerated by Abrupt Thaw Beneath Lakes," *Nature Communications* 9 (2018): 3262, https://doi.org/10.1038/s41467-018-05738-9.

102. S. Holm, J. Walz, F. Horn, et al., "Methanogenic Response to Long-Term Permafrost Thaw Is Determined by Paleoenvironment," *FEMS Microbiology Ecology* 96 (2020): fiaa021, https://doi.org/10.1093/femsec/fiaa021.

103. K. Schaefer, T. Zhang, L. Bruhwiler, and A. P. Barrett, "Amount and Timing of Permafrost Carbon Release in Response to Climate Warming," *Tellus Series B: Chemical and Physical Meteorology* 63 (2011): 168–180, https://doi.org/10.1111/j.1600-0889.2010.00527.x.

104. K. Walter Anthony, R. Daanen, P. Anthony, et al., "Methane Emissions Proportional to Permafrost Carbon Thawed in Arctic Lakes Since the 1950s," *Nature Geoscience* 9 (2016): 679–682, https://doi.org/10.1038/ngeo2795.

105. K. M. Walter, M. E. Edwards, G. Grosse, S. A. Zimov, and F. S. Chapin, "Thermokarst Lakes as a Source of Atmospheric CH_4 During the Last Deglaciation," *Science* 318 (2007): 633–636, https://doi.org/10.1126/science.1142924.

106. J. C. Aciego Pietri and P. C. Brookes, "Relationships Between Soil pH and Microbial Properties in a UK Arable Soil," *Soil Biology and Biochemistry* 40 (2008): 1856–1861, https://doi.org/10.1016/j.soilbio.2008.03.020.

107. S. Qiu, X. Zhang, W. Xia, et al., "Effect of Extreme pH Conditions on Methanogenesis: Methanogen Metabolism and Community Structure," *Science of the Total Environment* 877 (2023): 162702, https://doi.org/10.1016/j.scitotenv.2023.162702.

108. M. Fritz, J. E. Vonk, and H. Lantuit, "Collapsing Arctic Coastlines," *Nature Climate Change* 7 (2017): 6–7, https://doi.org/10.1038/nclimate3188.

109. H. Lantuit, D. Atkinson, P. P. Overduin, et al., "Coastal Erosion Dynamics on the Permafrost-Dominated Bykovsky Peninsula, North Siberia, 1951–2006," *Polar Research* 30 (2011), https://doi.org/10.3402/polar.v30i0.7341.

110. H. Lantuit, P. P. Overduin, and S. Wetterich, "Recent Progress Regarding Permafrost Coasts," *Permafrost and Periglacial Processes* 24 (2013): 120–130, https://doi.org/10.1002/ppp.1777.

111. P. P. Overduin, M. C. Strzelecki, M. N. Grigoriev, et al., "Coastal Changes in the Arctic," *Geological Society of London, Special Publication* 388 (2014): 103–129, https://doi.org/10.1144/SP388.13.

112. F. Giest, "Carbon Storage, Carbon Degradation and Sediment Transport Mechanisms in a Changing Coastal Thermokarst Landscape—Case Study for a Land—Near Shore Transect in the Teshekpuk Lake Region, Alaska, USA" (master's thesis, University of Potsdam, Germany, 2024).

113. J. Rydberg, J. Klaminder, P. Rosén, and R. Bindler, "Climate Driven Release of Carbon and Mercury From Permafrost Mires Increases Mercury Loading to Sub-Arctic Lakes," *Science of the Total Environment* 408 (2010): 4778–4783, https://doi.org/10.1016/j.scitotenv.2010.06.056.

114. P. F. Schuster, K. M. Schaefer, G. R. Aiken, et al., "Permafrost Stores a Globally Significant Amount of Mercury," *Geophysical Research Letters* 45 (2018): 1463–1471, https://doi.org/10.1002/2017GL075571.

115. M. C. Jones, G. Grosse, C. Treat, M. Turetsky, K. W. Anthony, and L. Brosius, "Past Permafrost Dynamics Can Inform Future Permafrost

Carbon-Climate Feedbacks," *Communications Earth & Environment* 4 (2023): 272, https://doi.org/10.1038/s43247-023-00886-3.

Supporting Information

Additional supporting information can be found online in the Supporting Information section.